

Chapter 5

Ionized Carbon in the Galactic Plane

5.1 Introduction

Ionized gas in the Galactic plane can be studied using recombination lines of hydrogen, and carbon. These two sets of lines arise in physically different gas clouds. At low frequencies, the hydrogen lines arise in hot ($T_e \sim$ few thousands), relatively tenuous ($n_e \sim 2-10 \text{ cm}^{-3}$), fully ionized clouds (Hart & Pedlar 1976, Lockman 1916, Anantharamaiah 1985, Anish Roshi & Anantharamaiah 1997) whereas the carbon lines arise in cooler ($T_e \sim 20-100 \text{ K}$), partially ionized low-density ($n_e < 0.5 \text{ cm}^{-3}$) clouds (Pedlar *et al.* 1978, Sorochenko & Walmsley 1991, Payne, Anantharamaiah & Erickson 1994 (hereafter PAE94), Anish Roshi & Anantharamaiah 1997). It is useful to mention at this point that the cosmic abundance by number of carbon is $\frac{n_C}{n_H} = 3.3 \times 10^{-4}$ (Allele 1976) and that its ionization potential is 11.4 eV as compared to 13.6 eV for hydrogen. It is the fourth most abundant species after H, He and O. Because of its lower ionization potential, carbon can get ionized in regions where hydrogen can still be neutral and the region can remain relatively cool compared to the region where hydrogen is fully ionized. As mentioned before, the ISM seems to be populated by two types of CII regions with distinct physical properties and environs. The first type are the CII regions observed in higher frequency recombination lines and are associated with HII regions. One such region associated with W3 is discussed in Chapter 6. The second type are the CII regions associated with cold, neutral gas in the ISM, detected by low-frequency recombination lines such as those discussed in Chapter 3. Carbon in these regions is ionized by the background UV radiation field ($E \geq 11.4 \text{ eV}$). These regions are at a lower equilibrium temperature (10 - 100 K) and have a lower electron density ($< 0.5 \text{ cm}^{-3}$). The CII region observed towards Cas A is an example of this type and it was discussed in Chapter 4. Hollenbach *et al.* (1991, hereafter HTT91) discuss low-excitation PDRs which are illuminated by the interstellar far-ultraviolet radiation

field. They go on to say that most of the neutral matter in the Galaxy is collected in the form of PDRs. From an **observational** point of view, it **appears** that at frequencies > 1.4 GHz or so (*i.e.* $n = 166$), one detects the C II region associated with H II region whereas at lower frequencies (all the way to $\nu \sim 15$ MHz & $n \sim 200 - 750$), the C II region associated with the cold neutral medium (CNM) of the ISM are detected. However, lines due to transitions near $n=166$ in carbon have been observed from both types of C II regions.

The Galactic plane, especially the inner regions of the Galaxy ($l < 20^\circ$) has been found to be widely detectable in low-frequency (< 500 MHz) recombination lines of carbon. Carbon lines have been observed towards the Galactic centre in emission at frequencies close to 408 MHz (Pedlar *et.al.* 1978) & 328 MHz (Anish Roshi & Anantharamaiah 1997) and in absorption near 76 MHz (Erickson, McConnell & Anantharamaiah 1995, hereafter EMA95) & 42 MHz (Smirnov *et.al.* 1996). Similar result has been obtained towards M16 also (Anantharamaiah, Payne & Erickson 1988). Extensive observations of the Galactic plane in carbon lines at 76 MHz made with the Parkes telescope have yielded positive results towards all the observed positions in the inner Galaxy ($l < 20^\circ$) (EMA95). The emission counterparts of some of these lines can be identified in the earlier observations at 328 MHz with the Ooty Radio Telescope (Anantharamaiah 1985). Carbon lines near 25 MHz have been observed from the direction of the galactic longitude of 75° and NGC2024 (Konovalenko 1984) and towards L1407, DR 21 & S140 (Golykin & Konovalenko 1990). Typical temperatures and densities that have been deduced for these partially ionized regions appear to match those of the neutral gas (atomic or molecular) in the Galaxy. However, detailed physical properties of the ionized gas and its association with the neutral gas components needs to be further explored.

In the present work, approximately 35 positions in the Galactic longitude range $342^\circ - 0^\circ - 145^\circ$ at Galactic latitude, $b = 0^\circ$ were observed in carbon recombination lines at 34.5 MHz using the low-frequency array at Gauribidanur. The observable positions were limited by the transit nature of the Gauribidanur telescope. Within the declination range of the Gauribidanur telescope, the particular positions that were selected were determined partly by the strong Galactic background in the inner Galaxy and partly by the positive results of other low-frequency observations. The main objective of the present study is to understand the distribution and physical parameters of regions of ionized carbon which are observed in RRL at very low frequencies. In the Galactic plane, we detected carbon lines from eight of the directions that were observed with the Gauribidanur telescope. In addition to these positions, carbon lines were also detected

from DR 21 and **Cas A**. A detailed list of **sources** and results of these observations **have** been tabulated in Chapter 3. The observations at **34.5 MHz** were supplemented by observations at **328 MHz** using the **Ooty Radio Telescope (ORT)**, where the absorption lines turnover into emission features. In this chapter, we attempt to obtain constraints on the physical parameters of the **region** which are responsible for the detected **lines**.

Unlike the direction **towards Cas A** which was discussed in the previous chapter, the observed line-to-continuum ratio at different frequencies towards various positions in the Galactic plane does not give the actual **line** optical depth at that particular frequency. This **is** due to the unknown size of the line-producing region. This uncertainty affects the interpretation and hence it is important to obtain a preliminary handle on the angular size of the **ionized** gas. For this purpose, we **conducted** observations with the ORT using two different angular resolutions (**2° x 6'** and **2° x 2"**) as described in Chapter 3. Comparison of the integrated line strength observed with the two different angular resolutions provided information on the size of the emitting region. Furthermore, an attempt was made using the VLA to map the carbon line emission near 332 MHz towards the position **G14+00** to obtain a more detailed knowledge of the spatial distribution.

In the following sections, the interpretation of the results of these observations is presented. Wherever possible, the results of the observations near 75 MHz (**EMA95**), 25 MHz (Konovalenko 1984, Golyнкин & Konovalenko 1990) and other existing data are used in the interpretation to obtain better constraints **on** the parameters.

5.2 The Angular Size of the Line-producing Clouds

Since the interpretation of the observed recombination lines in terms of the physical properties of the gas in which they arise depends sensitively on the fraction of the beam that is filled by the thermal gas, it is necessary to obtain a preliminary idea of its angular distribution. Our **observations** have been made at different **angular resolutions** ranging from **21' x 25"** at 34.5 MHz to **2° x 6'** at 328 MHz and **we** also make use of the **line** data at 76 MHz (**EMA95**) with a resolution of **4° x 4"**. **Unless the line radiation fills** the beam or the distribution of the continuum **intensity** is highly concentrated (like towards **Cas A**), beam dilution effects will be significant, **and** the actual line optical depths will be very different from the apparent (observed) optical depths. Therefore, before using the available low-frequency recombination line data to model the line-producing regions, it is essential to estimate the extent of this region. With this in mind, **we** observed some of the positions in the Galactic plane **at** 328 MHz using the ORT in its two separate

modes of operation **resulting** in different angular **resolutions**. The positions which were detected at **328 MHz** with a $2^\circ \times 6'$ beam **were** further investigated with a $2^\circ \times 2^\circ$ beam of **the** ORT. Comparing the integrated strength ($\int \frac{T_l}{T_{sys}} d\nu$) of the lines recorded during the two sets of observations, we can obtain constraints on the extent of the line-emitting region. Table 5.1 gives the the integrated line strengths ($\frac{\int T_l d\nu}{T_{sys}}$) observed using the two resolutions. Within the errors, the integrated line strengths are almost equal. It is, therefore clear from Table 5.1, that the angular extent of the cloud giving

Table 5.1 Integrated carbon line ($n \sim 271$) strengths with two different beams used in the ORT observations at 328 MHz.

No.	Source	$2^\circ \times 6'$	$2^\circ \times 2^\circ$
		$A = \frac{\int T_l d\nu}{T_{sys}}$ s^{-1}	$B = \frac{\int T_l d\nu}{T_{sys}}$ s^{-1}
1	G352+00	5.1(2.5)	6.9(0.7)
2	G00+00	14.8(1.8)	13.5(1.8)
3	G05+00	10.9(0.9)	9.8(0.6)
4	G10+00	13.7(1.1)	10.7(1.0)
5	G14+00	18.8(1.2)	12.7(4.1)
6	G16.5+0	6.5(0.8)	7.0(0.6)

rise to low-frequency carbon line emission near $n=271$ in the inner Galaxy is $\geq 2^\circ$ for most of the lines of sight. For G10+00 and G14+00, the region appears to be slightly smaller than 2° . Although the overall angular extent of the line-emitting regions could be large, the region could be made of a number of nearly uniformly distributed clumps in the field of view. This scenario is not ruled out **from** the constraints imposed by the observations at **328 MHz using** the ORT. **To** obtain further **constraints** on the **clumpiness** of the emitting regions, **we** mapped a 2° region around G14+00 in C270 α using the VLA with a resolution of $\sim 4'$. **Although** the **observations** were severely affected by interference and other problems leading to **low-sensitivity** **and** no detection of carbon lines, a comparison of the results **from** ORT with the limits derived from these observations indicates that the line-emitting region towards G14+00 is larger than $10'$. The arguments are **as** follows. The strength of the carbon line detected by Anantharamaiah (1985) at **328 MHz** with a $2^\circ \times 6'$ beam is **160 mJy**. The **3 σ** limit on the detection in the line images of G14+00 obtained using the VLA is **75 mJy/beam** (**beam**= $5.4' \times 3.5'$) (see Chapter 3). If the line detected with the ORT was confined to

about 2 VLA beam areas **then** the line would have been detected with the VLA. In other words, since the region is larger than $\sim 10'$, the sensitivity of the VLA observations have failed to detect the line. In the present work we, thus, assume that the ionized carbon gas in the **inner** Galaxy is distributed in clouds of size either 2° or more.

From their observation of carbon lines near 76 MHz as a function of Galactic latitude, **EMA95** concluded that the line-forming region in the inner Galaxy must be approximately 4° wide in latitude. Similarly very low-frequency (near 25 MHz) observation towards $l = 75^\circ$ in the Galactic plane (**Konovalenko** 1984) has indicated that the carbon line-producing region $\geq 4^\circ$ in extent.

It, therefore, appears that the ionized carbon regions sampled by the low-frequency recombination **line** observations are at least a few degrees in extent.

5.2.1 Beam Dilution at 34.5 MHz

An important point to consider from the conclusion in the previous section concerning the angular dimensions of the emitting region is the beam dilution for the carbon lines observed at decametre wavelengths. The **E+W** arm of the Gauribidanur telescope has **an** angular resolution of $21' \times 25^\circ$ ($a \times b$). Although this is a large beam in the north-south direction, the extent to which beam dilution occurs depends both on the continuum emission within the beam and the angular **size** of the line region. Since the total system temperature is dominated by the sky background, if both the line and continuum emissions are distributed over the same area of the beam again there is no beam dilution. Similarly, if the continuum emission is strong and confined to a region **as** small **as** or smaller than the **absorbing** cloud, then there is no beam dilution. However, if the continuum emission **covers** the entire beam and the line emission is confined to a smaller area, beam dilution will lead to a reduction in the line-to-continuum ratio. In Fig 5.1, we have shown the one-dimensional continuum brightness distribution across the length of the Gauribidanur beam ($21' \times 25^\circ$) when pointed towards **G00+00**, **G16.5+00**, **G63+00** and **G75+00**. The brightness distribution was obtained from the “**all-sky**” continuum map at 34.5 MHz made using the Gauribidanur array by **Dwarakanath** (1989). The brightness distribution towards the Galactic centre (see Fig 5.1 (a)) and also towards **G05+00** is not uniform over the entire stretch of the beam but is peaked sharply at the center. In the **rest** of the positions towards which carbon lines have been detected, **such strong peaks** in the continuum is not seen as evident from Fig 5.1 (b) to (d). Therefore, unless the line emission is **also** distributed over the entire 25° beam, the brightness distribution shown in these figures indicates that the line emission will be beam-diluted. If the line region **has** an angular extent of $2^\circ - 4''$

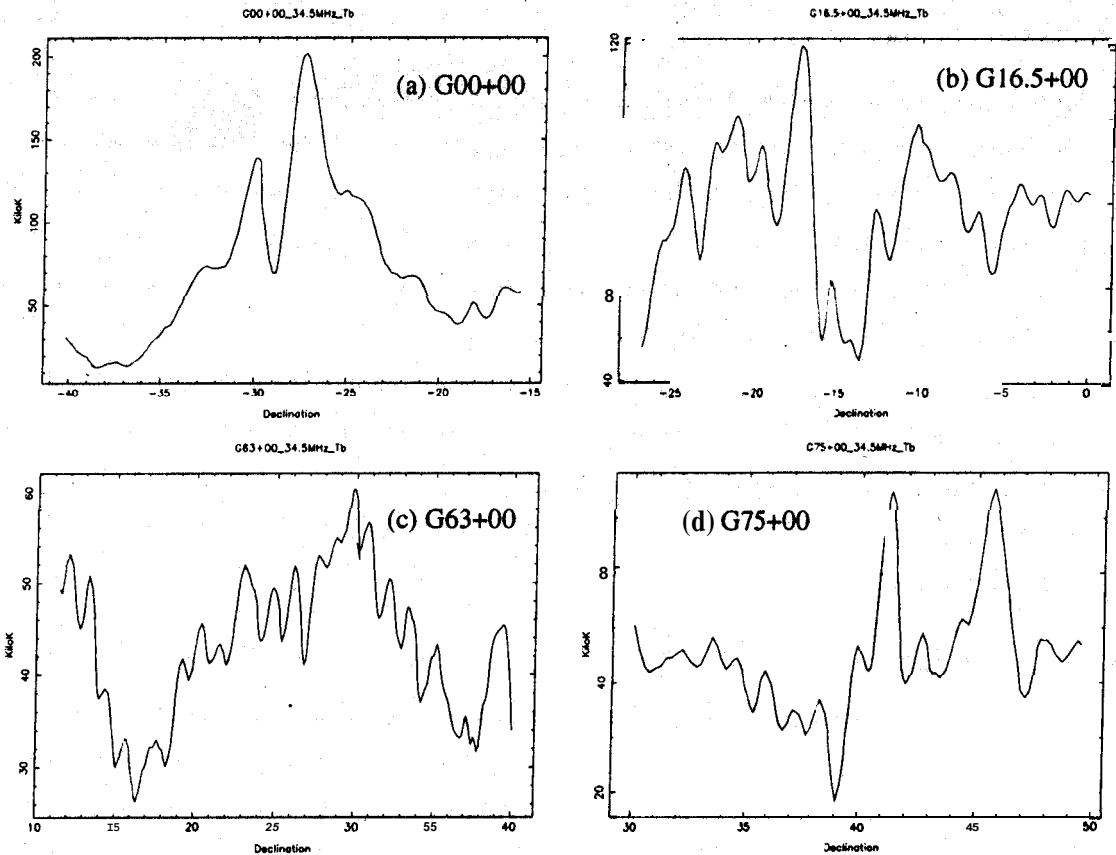


Figure 5.1 One-dimensional brightness distribution at 34.5 MHz across the **E+W** arm total power beam ($21' \times 25'$) near the Galactic Centre (a), **G16.5+00** (b), **G63+00** (c) and **G75+00** (d) obtained with an angular resolution of $26' \times 42'$ (from Dwarakanath 1989)

about the Galactic plane then the beam dilution factors for the absorption feature at 34.5 MHz range from 0.1 to 0.2. It **should**, however, be noted that the possibility of the thermal gas filling the entire **Gauribidanur telescope beam** and hence leading to a beam dilution factor of unity cannot be conclusively ruled out. Towards the Galactic centre and **G05+00**, the continuum falls **off** rather steeply, by almost a factor of two, outside a 10° region. The effective beam dilution will therefore be smaller for these directions.

5.3 Constraints from the Observed Line Widths

One notable difference between the carbon lines observed towards Cas A and the lines observed from positions in the Galactic plane is the width of the lines. While the lines detected towards Cas A are seen to broaden with increase in quantum number which is a clear indication of pressure & radiation broadening, no such trend is seen in the

lines observed from the Galactic plane.

Table 5.2 Widths of the carbon recombination lines observed at 25 MHz, 34.5 MHz, 42 MHz, 76 MHz and 328 MHz

No.	Position	$\Delta V \text{ kms}^{-1}$			
		n~686 25 MHz	n~575 34.5 MHz	n~443 76 MHz	n~271 328 MHz
1	G352+0	-	36.4 ± 3.6	11 ± 1	20.1 ± 1.7 (G355+00)
2	G00+00	-	20.5 ± 1.2	24 ± 1	27.0 ± 1.5
3	G05+00	-	21.0 ± 2.5	25 ± 4 (G06+00)	16.2 ± 0.9
4	G10+00	-	37.0 ± 3.2	26 ± 2	36.3 ± 2.9
5	G14+00	-	56.0 ± 4.5	25 ± 3	54.6 ± 8.7
6	G16.5+0	-	32.6 ± 3.4	47 ± 4	12.7 ± 2
7	G63+00	-	45.9 ± 4.4	-	-
8	G75+00	15 ± 0.9	24.4 ± 2.8	-	-
9	DR21	42 ± 12	18.5 ± 2.7	-	-
10	Cas A	71.9 ± 16.4	26.0 ± 3.1	6.7 ± 0.4	5.0 ± 0.5

The widths of the lines observed at 25 MHz, 34.5 MHz, 76 MHz and 328 MHz from various positions in the Galactic plane are given in Table 5.2. Within the errors, the observed widths at all the four frequencies are **comparable**. The differences that are seen **can** be attributed to the **non-overlapping** portions of the beams at the **different** frequencies. In contrast, the line-widths observed at these frequencies in the direction of Cas A (see the last row of Table 5.2) **increase** sharply with the quantum number. The absence of similar line broadening towards the Galactic plane can be interpreted in terms of lower electron densities and weaker radiation field incident on the ionized carbon cloud in the Galactic plane as compared to that in the Perseus arm. The widths ($\sim 25 \text{ kms}^{-1}$) of the lines from **the** Galactic plane at all the observed frequencies are much larger than those expected from thermal and turbulent motions ($\sim \text{few kms}^{-1}$) in the clouds. These large widths **are** most likely due to systematic motions arising from differential Galactic rotation.

From the observed line widths at 34.5 MHz, we derive the upper **limits** on the electron density using Eqn 2.27 and upper limits on the radiation temperature using Eqn 2.29 for each of the Galactic plane position. These are listed in Table 5.3. The upper limits on the electron density in the medium were calculated **assuming** that the entire observed width is due to pressure broadening at a temperature of 20 K. Upper

limit on the radiation temperature at 100 MHz (T_{R100}) for the various positions was calculated assuming that the observed width is only caused by the incident non-thermal ambient radiation field. The observed width at 34.5 MHz translates to a upper limit for the kinetic temperature of $T_e < 10^5$ K.

Table 5.3 Upper limits on the electron density and radiation temperature (at 100 MHz) from the observations at 34.5 MHz

No	Source	Observed Line width kms ⁻¹	From ΔV of C575 α		Tb(25°) at 34.5MHz	
			$n_{e,max}$ ($T_e = 20$ K) cm ⁻³	$T_{R,max}$ (100 MHz) $W_\nu = 1$ K	T_R (100 MHz) a = 2.6 K	Expec ΔV $W_\nu = 1$ (34.5MHz) kms ⁻¹
1	G352+00	36.4(3.6)	1.21(0.12)	5160(510)	3460	24.4
2	G00+00	20.5(1.2)	0.68(0.04)	2906(170)	5030	35.5
3	G05+00	21.0(2.5)	0.7(0.08)	2977(354)	5030	35.5
4	G10+00	37.0(3.2)	1.23(0.11)	5245(454)	5660	40.0
5	G14+00	56.0(4.5)	1.86(0.15)	7938(638)	5660	40.0
6	G16.5+0	32.6(3.4)	1.08(0.11)	4621(482)	5030	35.5
7	G63+00	45.9(4.4)	1.51(0.15)	6507(624)	2830	20.0
8	G75+00	24.4(2.8)	0.81(0.09)	3459(370)	2830	20.0
9	DR21	18.5(2.7)	0.61(0.09)	2622(383)	2680	19.0

Columns 4 & 5 list the limits on n_e and T_{R100} derived from the linewidth near 34.5 MHz.

Column 6 lists the T_{R100} averaged over the Gauribidanur beam (25°) extrapolated from the continuum map at 34.5 MHz (Dwarkanath 1989).

Column 7 shows the expected line broadening at 34.5 MHz due to T_{R100} noted in column 6.

A beam dilution factor, $W_\nu = \Omega/4\pi = 1$ has been used - in reality it could be any number between 0 and 1 depending on the solid angle of the radiating source seen by the cloud of thermal gas.

Lack of strong dependence of line width on **frequency** indicates the insignificant contribution of pressure broadening at 34.5 MHz. Thus, the actual electron densities are likely to be much smaller than those listed in Table 5.3. Furthermore, the allowed electron density **decreases** if the kinetic **temperature** is increased *e.g.* the values of n_e noted in column 4 of Table 5.3 will decrease by a factor of ~ 4 for a T_e of 75 K. Similarly, since radiation broadening is not important near 34.5 MHz, the actual radiation field that illuminates the cloud is probably much weaker than that noted in column 5 of Table 5.3. The derived upper limit for the radiation temperature assumes a dilution factor of 1 which implies that the absorbing cloud is embedded in a non-thermal radiation field and isotropically illuminated by it. The actual radiation temperature

seen by the cloud could be equal to or less than the values listed in column 6 of Table 5.3, which were obtained from the 26' x 42' continuum map of **Dwarakanath (1989)**. The widths of the carbon lines near 34.5 MHz as predicted by this observed radiation field are listed in column 7. In some of the cases, the maximum allowed width due to radiation broadening is of the order of or larger than the observed width. Since radiation broadening contributes insignificantly to the linewidth at 34.5 MHz, the radiation field illuminating the clouds is much weaker than the values listed in column 6.

The limits listed in Table 5.3 are useful because they define the boundaries of the parameter space that is used for modelling the observed recombination lines.

5.4 Site of Origin of Low-frequency Recombination Lines

From the upper limits on the electron temperature and density obtained **from the** observed width of the **recombination** line at 34.5 MHz, it can be inferred that the lines can arise in either hot or cold tenuous gas. Considering the **various** components of **the ISM (McKee & Ostriker 1977 and Kulkarni & Heiles 1988)**, the observed lines can arise in either the warm ionized medium (WIM), the warm neutral medium (WNM), the cold neutral medium (CNM) or in molecular clouds. Cold neutral gas (atomic or molecular) is the favoured site of origin of these lines if they are of carbon and the hot tenuous gas is the favoured site if the lines are due to elements heavier than carbon *i.e.* Mg & Ca. Since the rest frequencies of the lines due to heavier atoms are separated from that of the carbon lines by a small amount ($\sim 6 \text{ kms}^{-1}$ in terms of velocity), **there** is ambiguity regarding their identification. Dielectronic-like recombination in carbon which leads to increased level populations at certain quantum numbers is an important process at temperatures typical of the CNM. As discussed in Chapter 4, inclusion of this process in the calculation of the departure coefficients has indeed explained the observed variation in the optical depths of the lines towards Cas A (Payne, Anantharamaiah & **Erickson 1989** (hereafter **PAE89**), **Sorochenko & Walmsley 1991, PAE94**). On the other hand, dielectronic recombination in elements like Mg and Ca which is effective at temperatures typical of the WIM & **WNM** can boost the level populations considerably, leading to observable lines despite the low elemental abundances (Shaver 1976, Blake, *et. al.* 1980, **Walmsley & Watson 1982**). These two possible sites of origin are discussed separately below:

5.4.1 Origin of Low-frequency lines in Hot Gas

When the first low-frequency recombination line was observed in absorption at 26.1 **MHz against Cas A** (Konovalenko & Sodin 1980), it was interpreted as being either due to carbon in neutral hydrogen clouds with temperature near 50 K and electron density of $< 0.1 \text{ cm}^{-3}$ or due to elements like magnesium and calcium arising in hot clouds at a temperature close to 10^4 K (Blake *et.al.* 1980). Shaver (1976) had shown that gas with cosmic abundances of heavy atoms at a temperature of $\sim 10^4$ K and electron density of $\sim 0.05 \text{ cm}^{-3}$ (typical of WIM) distributed over a **pathlength** of ~ 10 kpc can give rise to line-to-continuum ratios of a few times 10^{-4} because of increased level populations through dielectronic recombination. Even the turnover from emission to absorption with lowering of frequency is expected for the lines **arising** in this hot gas. However, this origin for the low-frequency recombination lines is not favoured because long path lengths are required to explain the observed line strengths. The lines seen towards Cas A arise in the Perseus arm which is at a distance of ~ 2.5 **kpc** from the solar **neighbourhood**. If these low-frequency lines were arising in the hot tenuous gas then such short pathlengths (< 2.5 kpc) would have made the lines undetectable. The fact that the strongest lines are observed from this direction strongly suggests that the origin of these low-frequency lines is not in the WIM or the WNM. Moreover, optical observations have shown that metals like Mg and Ca are heavily depleted in the ISM (Crinklaw *et.al.* 1994, Jenkins 1987) and hence the lines are expected to be **weak**. We should, however, keep in mind that the high-temperature models are not conclusively ruled out.

5.4.2 Origin of Low-frequency lines in Cold Neutral Gas

Here the term 'neutral' refers to both, the CNM *ie.* atomic HI gas and the molecular gas in the ISM. The low-frequency recombination lines observed towards the direction of Cas A and their interpretation has shown that these lines are due to ionized carbon in the neutral gas. If, as a first approximation, these regions in the Perseus arm are considered to be representative of the regions sampled by the **low-frequency radio recombination** lines, then the neutral gas is a highly likely site of origin of the carbon recombination lines from the Galactic plane.

However, the difference in the effect of pressure and radiation broadening on the low-frequency line profiles observed towards Cas A and towards other positions in the Galactic plane suggests that detectable **low-frequency** lines may arise in regions with a range of physical properties, not unlike the neutral gas. In a recent review, Sorochenko

(1996) discusses **Cas A** and other such directions towards which carbon lines have been detected and concludes that the **C II** regions are formed on the surface of molecular clouds exposed to external ionizing UV radiation either close to **H II** regions or around isolated molecular clouds.

It thus appears that there is sufficient evidence to regard the cold neutral gas (atomic or molecular) as the site of origin of low-frequency carbon lines. In the following three sections, we discuss the possible association of the carbon line-emitting regions in the **Galactic** plane with **H I** or **H₂** gas using the **l-v** diagram and other observed parameters of the lines.

5.4.3 The Longitude-Velocity Diagram of Carbon Recombination Lines at 34.5 MHz & 328 MHz and Comparison with **H I** & **¹²CO**

The **l-v** diagram shown in Fig 5.2 is obtained by plotting the longitude at which the observation is made against the radial velocity extent of the spectral line. If a cloud at a particular longitude is participating in Galactic differential rotation, then only a certain range of velocities are allowed to it. Gas which is close to the sun is expected to lie close to the zero **radial** velocity axis. In Fig 5.2, the radial velocities of carbon lines observed both at 34.5 MHz and 328 **MHz** are plotted. The line segments drawn parallel to the x-axis about the observed point represents the width of the line **as** listed in Table 5.2.

The nature of the expected **l-v** curve for Galactocentric distances of 7.5 kpc and 4 kpc using the Galactic rotation model of Burton (1988) are shown as the solid and dashed lines respectively in Fig 5.2. All the gas in the inner Galaxy that produce the carbon line at 34.5 MHz and 328 MHz **seems** to lie within this range which coincides with the ring of material in the inner Galaxy containing high surface densities of molecular clouds (Scoville & Solomon 1975) and **H II** regions. Part of the line intensity observed towards **G63+00** also seems to lie in this range, However, the gas sampled towards the position **G75+00** lies well outside the 4 – 7.5 kpc range and appears to be in the solar neighbourhood. Our results are similar to that of **EMA95** who surveyed the inner Galaxy in carbon recombination lines at 76 MHz using the Parkes telescope. They found that the gas giving rise to the lines near 76 MHz lies between 5 kpc and 8 kpc. These results indicate that the emission lines observed near 328 MHz and the absorption lines detected near 34.5 MHz and 76 MHz from the inner Galaxy ($l < 20^\circ$) originate in the same gas.

The radial velocities of the carbon lines observed at 34.5 **MHz** and 328 MHz **from** various positions in the Galactic plane do not show perfect correspondence (see Table

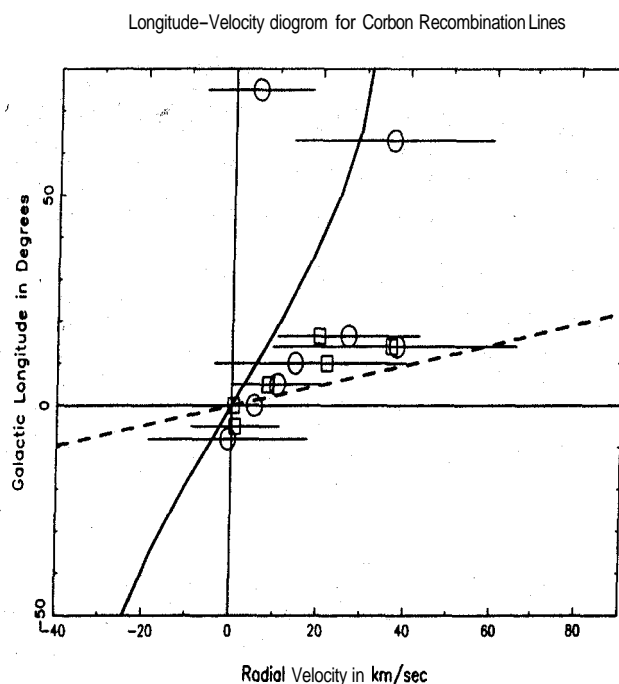


Figure 5.2 The Longitude-Velocity diagram of the carbon recombination lines at 34.5 MHz(**circles**) and 328 MHz(**squares**) from the Galactic plane. The horizontal lines about each point represent the observed widths of the lines. The solid line shows the variation of the radial velocity with longitude for gas at a Galactocentric distance of 7.5 kpc whereas the dashed line shows the expected l-v plot for gas at a distance of 4 kpc. These are obtained using the Galactic rotation model of Burton (1988).

5.4). 'As seen in Table 5.4, the difference in radial velocities at the two frequencies ranges **from** 1 to 7 kms^{-1} . This discrepancy can be attributed to the different **angular** resolutions of the two observations. We also compared the line velocities at these frequencies with those at 76 MHz (**EMA95**). From Table 5.4, we note that the difference in radial velocities of the three lines is maximum **for G14+00**. The difference for **G352+00** and **G16.5+00** is also considerable. Again, the non-overlapping regions of the beams are probably responsible for these differences.

Comparing the l-v diagram for carbon **lines** detected at 34.5 MHz and 328 MHz with that of HI, we find **that** the carbon lines are observed over a narrower range of velocities as compared to HI emission. This is not surprising because both the **CNM** and WNM with their widely-different physical conditions contribute to the observed HI emission. In fact, HI emission is detected at all velocities that are allowed by Galactic rotation. On the other hand, the carbon recombination lines are likely to arise only under certain physical conditions; if the **gas** in the Perseus arm towards **Cas A** is a prototype C II region, then **gas** at 50 – 100 K and electron densities $< 0.1 \text{ cm}^{-3}$

Table 5.4 The radial velocities of the carbon recombination lines observed at various frequencies. A dash indicates that no data is available at that frequency.

No.	Position	$V_{lsr} \text{ kms}^{-1}$			
		n~686 25 MHz	n~575 34.5 MHz	n~443 76 MHz	n~271 328 MHz
1	G352+0	-	-0.8 ± 1.5	-10	0.8 ± 0.7 (G355+00)
2	G00+00	-	5.2 ± 0.5	-1	0.5 ± 0.6
3	G05+00	-	10.3 ± 1.0	9 (G06+00)	8.2 ± 0.4
4	G10+00	-	14.4 ± 1.3	17	21.7 ± 1.2
5	G14+00	-	37.7 ± 1.9	16	36.5 ± 3.7
6	G16.5+0	-	26.6 ± 1.4	14	20.0 ± 0.8
7	G63+00	-	36.4 ± 1.9		-
8	G75+00	11.0 ± 0.4	5.5 ± 1.2		-
9	DR21	0 ± 0.8	4.4 ± 1.1	-	-

is the favoured site of origin of these lines. In Table 5.5, the range of velocities over which HI emission, HI absorption, $C575\alpha$ and ^{12}CO have been detected are tabulated for different positions. Data on HI emission were taken from the l-v diagrams given in Burton (1988). The ^{12}CO spectra towards longitudes $=14^\circ, 16.5'$ were taken from Cohen (1986) which had a velocity coverage of $\sim 150 \text{ kms}^{-1}$ and those towards $l=0^\circ, 5^\circ, 10^\circ, 63^\circ, 75^\circ$ were obtained from observations using the 10.4 m telescope at Raman Research Institute with a velocity coverage of 300 kms^{-1} . The data towards G352+00 was taken from Bania (1977) which had a velocity coverage of 600 kms^{-1} . The bandwidth used for the Gauribidanur recombination line observations was 250 kms^{-1} . Except for G352+00 and G00+00, the molecular gas seems to be confined to a narrower range of velocities like the recombination line and in most cases, the velocities of recombination lines are a subset of or of the order of the molecular line velocities. This maybe indicative of a correlation between the two regions. In the case of G63+00 and G75+00, the recombination line spans a wider velocity range than the molecular line. In Fig 5.3, $C575\alpha$, 21-cm HI emission, 21-cm HI absorption and ^{12}CO emission spectra towards G10+00 are shown on the same velocity scale. The ubiquity of HI seen in emission and the narrow range of velocities over which HI absorption and carbon recombination lines are seen is evident. HI observed in absorption preferentially samples the lower

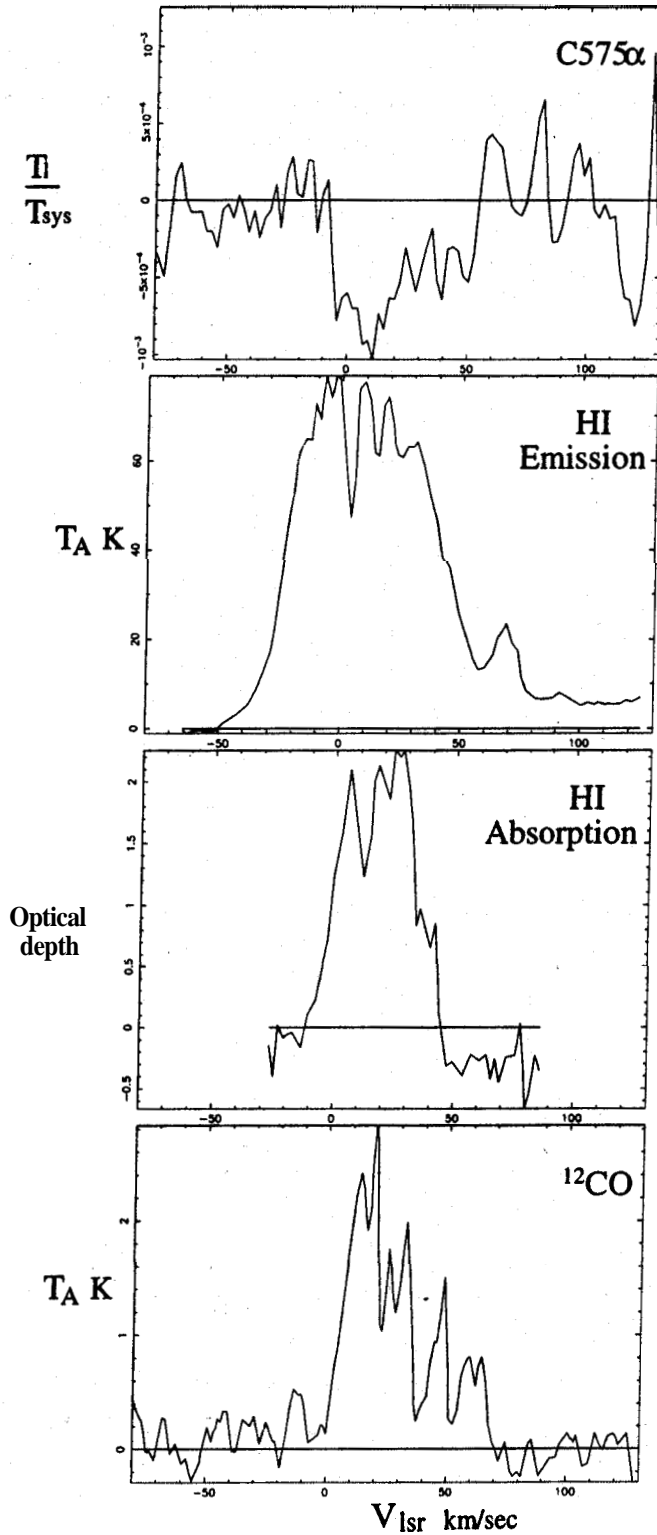


Figure 5.3 C575 α , HI 21-cm emission, HI 21-cm absorption and ^{12}CO spectra in the direction of G10+00 showing the velocity coverage of line features.

temperature gas. For positions towards longitudes of 352° , 0° , 10° , $16.5''$ and $63''$, HI absorption measurements towards continuum sources which were located within the $2''$ region defined by the ORT beam were obtained and are listed in columns 5 & 6 of Table 5.5. For the other positions, the continuum source towards which absorption

Table 5.5 Comparison of the range of radial velocities over which HI, C575 α & ^{12}CO are observed.

No.	Long	HI				C575 α		^{12}CO	
		Emission		Absorption		V_{min} kms $^{-1}$	V_{max} kms $^{-1}$	V_{min} kms $^{-1}$	V_{max} kms $^{-1}$
		V_{min} kms $^{-1}$	V_{max} kms $^{-1}$	V_{min} kms $^{-1}$	V_{max} kms $^{-1}$				
1	352°	-225	60'	-106	4	-18	18	-100	10
2	0°	-250	125	-108	67	-5	15	-50	130
3	$5''$	-75	200	3	18	0	20	0	30
4	10°	-50	175	5	35	-5	30	0	70
5	14°	-50	150	3	27	10	65	0	70
6	16.5°	-50	150	-2	24	10	44	10	70
7	$63''$	-125	50	-74	41	15	60	-13	31
8	$75''$	-100	45	-	-	-7	18	-5	5

had been detected were in the same **general** direction but lay outside the ORT beam. These are **also** noted in Table 5.5. The HI absorption data towards $l=5^\circ$, 10° , 14° and $16.5''$ were taken from the observations of Radhakrishnan *et al.* (1972) which had a velocity coverage of 135 kms^{-1} . Data for G352+00, G00+00 and G63+00 were taken from Garwood & Dickey (1989, hereafter GD89) and had a velocity coverage of 660 kms^{-1} . The absorption lines of HI are generally narrow and on the average, many distinct features are detected within the range noted in the Table. For simplicity in comparison, we have noted only the range of velocities and not the individual components. The velocity range of the HI absorption features correspond well with the recombination line features in many cases. However, like ^{12}CO , the HI absorption features are observed over a wide range of velocities for G352+00 and G00+00 of which the carbon recombination line velocities form a subset. Thus, it appears that carbon recombination lines, the HI gas seen in absorption and the molecular gas share similar radial velocity characteristics suggesting physical proximity. However, it is difficult to differentiate between the association of ionized carbon with either atomic or molecular gas, in general, and **from** our observations in particular, as the following discussion highlights.

Various studies concerning the physical association between the cold, atomic absorb-

ing gas and the molecular gas have been conducted. **Kazes & Crovisier (1981, hereafter KC81)** find that, although there is good correlation between the radial velocities of the CO lines and the HI absorption lines, no correspondence between the HI optical depths and CO emission line intensities is discernible. This is also observed by GD89 in their sample. On the basis of the line parameters (other than the radial velocities), KC81 rule out correlation between the two. Contrary to this viewpoint, GD89 argue that the lack of further correlation between the atomic and molecular lines as being due to CO radiative transfer effects and temperature variations in the molecular gas which are distinct from that of the atomic gas. Hence they explain that, except for the radial velocities, no other similarity in the lines of the two species from physically close clouds are to be expected.

All the cold atomic gas seen in absorption is expected to have GO emission counterparts (Burton & Gordon 1978), although the exact spatial correspondence between the two is not clear. Despois & Baudry (1985, hereafter **DB85**), in an extensive comparison, find that less than 20 % of HI absorption features have a CO counterpart. Moreover for these 20 % **cases**, no correlation of CO intensities with parameters derived from the HI absorption line is seen **as** also noted by GD89 and **KC81**. On the other hand, GD89 find from their sample that 85 % of the directions which show HI absorption with an optical depth > 0.1 also show CO emission. The main difference between the two studies, which is probably responsible for the different results is that DB85 include many lines-of-sight with latitudes $> 1^\circ$ whereas GD89 study focusses only on HI absorption closer to the plane at latitudes $< 1^\circ$. Tight association between the atomic and molecular gas exists within the solar circle where molecular gas is found in abundance. GD89 infer from their HI absorption measurements **close** to the Galactic plane that there is less atomic absorbing gas at small Galactocentric radii than in the solar neighbourhood **inspite** of the increase in the surface density of molecular gas in the central Galactic regions. Hence, if the gas which is observed in low-frequency carbon recombination lines is coexistent with the absorbing atomic gas, then it is likely to be located in the solar neighbourhood whereas if it is coexistent with molecular gas, then probably located at **smaller** Galactocentric distances. It may be **useful** to note that if carbon recombination lines arise in gas located in the solar **neighbourhood** then clouds of even small linear dimensions can **subtend** large angles at the radio telescope.

From the above discussion, we can say that the carbon recombination line emission is associated with either the cold atomic gas or the molecular gas in the Galaxy. It is difficult to distinguish between atomic and molecular gas **as** the site of origin of low-frequency carbon recombination lines on the basis of observed radial velocities.

Furthermore, both the sites are considered to have favourable physical conditions for the production of carbon lines. The proximity of the two components *i.e.* H_2 & HI (as discussed above) introduces further uncertainty in establishing the site of origin of these lines. Since the cold atomic gas and molecular gas are intimately related within the solar circle in the Galactic plane, as the study by GD89 shows, whatever results we discuss here may have this inherent uncertainty. This uncertainty is difficult to remove unless **carbon** lines are detected from a direction where either only HI is observed in absorption or only ^{12}CO is detected. As of now we do not have such a detection and hence we suggest it as a possible future work to enhance our knowledge of ionized carbon regions in the **ISM**.

5.4.4 The Line-to-Continuum Ratios of Carbon Recombination line & Comparison with HI & ^{12}CO

In this subsection, we examine any possible correlation between the intensity of low- v carbon recombination lines and the observed HI optical depth in that direction & also the intensity of ^{12}CO lines. HI optical depths in the inner Galactic plane is found to vary between 0.1 to 2.5 (GD89) with most features having an optical depth between 0.5 to 1. We can **infer** from the available data that in many cases (*e.g.* **G352+00**, **G00+00**, **G05+00**), carbon recombination lines are detected close to the velocities at which the largest optical depth in HI (~ 1) is observed towards that direction. However, if the correlation between the optical depths of 21-cm HI and low- v carbon lines was strong, then we should have detected carbon lines from many more directions in the Galactic plane. For example, although $\tau_{\text{HI}} > 3$ towards G30.8-0.0 (Radhakrishnan *et al.* 1972), we **fail** to detect any carbon line at 328 **MHz** towards this direction; the upper limit to the line-to-continuum ratio being 2.6×10^{-4} . No recombination lines have been detected towards the extragalactic source **3C123** to an optical depth limit of 3×10^{-4} although HI optical depth is very high in that direction (Payne, Salpeter & Terzian 1984). Absence of easily-detectable lines from such directions suggests that the afore-mentioned correlation may be a coincidence or that other factors may also be at play. The latter **seems** to be the case since carbon lines are detected near the velocities of the deepest HI feature within the range noted in Table 5.5 in many of the positions. We also tried **to** see if the carbon recombination lines are observed at velocities at which ^{12}CO emission **peaks**. In Table 5.6, the radial velocities at which HI absorption **has** maximum optical depth and ^{12}CO has highest emission are listed alongwith the velocities at which peak line-to-continuum ratio of recombination lines is recorded.

Table 5.6 Comparison of the radial velocities of peak $Cn\alpha$, HI absorption & ^{12}CO

No.	Position	$V_{\text{lsr}} \text{ kms}^{-1}$				
		n~575 34.5MHz	n~443 76MHz	n~271 328MHz	HI Abs 1.4GHz	^{12}CO 115GHz
1	G352+0	-0.8	-10	0.8	-8, -48, -35	-45, -80
2	G00+00	5.2	-1	0.5	0, 67, 11	-20
3	G05+00	10.3	9	8.2	7, 18	12
4	G10+00	14.4	17	21.7	25, 15, 10	16
5	G14+00	37.7	16	36.5	20, 5	20, 45
6	G16.5+0	26.6	14	20.0	6, 2, 20	30, 45
7	G63+00	36.4	-	-	-6, 25, 11	-11, 28
8	G75+00	5.5	-	-	5	0.5
9	DR21	4.4	-	-	-	-3, 11

Column 3 lists the peak radial velocities observed by us at 34.5 MHz.

Column 4 lists the peak velocities for lines near 76 MHz observed by EMA95.

Column 5 lists those for lines near 328 MHz observed by us.

Column 6 lists the velocities of peaks of HI optical depth. The listed **numbers** in a line are in decreasing order of the HI optical depth. The data for **G05+00, G10+00, G14+00, G16.5+00** are taken from Radhakrishnan (1972) & **G352+00, G00+00** and **G63+00** are taken from Garwood & Dickey (1989).

Column 7 lists the peak emission velocities of ^{12}CO for **G352+00** taken from Bania (1977), for **G14+00 & G16.5+00** taken from Cohen (1986) and **G00+00, G05+00, G10+00, G63+00, G75+00** from our observations. For DR 21, the ^{12}CO data is from Richardson *et.al.* 1986.

We can infer from Table 5.6 that except for the position **G05+00**, there does not seem to be a tight correlation between the peak velocities of atomic and molecular gas and the recombination lines. One reason for this is the somewhat different radial velocities of the peak line-to-continuum ratio of recombination lines at 34.5 MHz, 76 MHz and 328 MHz. Hence, although a carbon line at one of the frequencies is detected close to the velocity at which the deepest HI feature is observed within the range noted in Table 5.5, there is difference in the observed **velocities**. The obvious conclusion one can draw from this is that the carbon line-forming **gas** is not necessarily coexistent with the strongest atomic or molecular gas concentrations. However, this may not be correct and the answer to the discrepancy may possibly lie in the influence of other factors such as the physical properties of the cold clouds, their beam-covering factor and the fraction of carbon that is depleted onto grains, The neutral gas observed towards different directions can possess a range of physical conditions and all of which

may not be conducive to formation of low-frequency carbon recombination lines or rather, of detectable low-frequency **lines**. Another possible reason for the absence of correlation could be the cloud size. At long wavelengths, practical reasons restrict spatial resolutions and sensitivities and it is difficult to obtain the dimensions of the line-forming region. Since the cloud could be of any size ranging from a small fraction of the beam to the size of the entire beam or even larger, it will **strongly influence the** detectability of the line. The third factor that may influence the **detectability** of the line is the **fraction** of carbon that is depleted onto grains. In addition to reducing **the column density of** ionized carbon in a cloud, depletion **of** carbon may **affect** the level population in high quantum states as described in the next section. Thus, since the detection of the carbon lines depends on many properties of the medium, absence of a direct correlation **between** the observed HI optical depths, ^{12}CO intensities and detectable carbon lines may not be surprising.

We now turn to modelling of the recombination line-forming region to obtain constraints on the physical properties such as temperature, density and emission measure.

5.5 Modelling the Line-Forming Regions

In the above sections, **we** have **discussed** the possible association of ionized carbon gas with cold atomic hydrogen and molecular gas as deduced from a comparison of the observed line strengths and radial velocities. This type of analysis **can**, at best, give only a rough idea of the physical proximity of the different species and hence the probable range of physical parameters. To derive quantitative estimates of the physical parameters in the ionized carbon regions, rigorous modelling is required. In this section, we model the ionized carbon regions which are detected in our observations. In addition to the data obtained here at 34.5 MHz and 328 MHz we also use other **low-frequency** recombination line data that is available in the literature. For regions in the inner Galaxy, we use the data at 76 MHz obtained by EMA95 using the **Parkes** 64-m radio telescope in Australia. All the clouds **along** the line of sight are assumed to be isothermal and homogeneous. We begin with a description of the physics underlying the modelling and then go on to the actual modelling procedure, the criteria used to select the favourable models and finally the results of the modelling are presented.

5.5.1 Physics underlying the modelling

Since the physics of recombination lines have already been discussed in Chapter 2, here we only present the relevant equations used in the modelling and the assumptions made

before using these equations.

The solution to the radiative transfer equation (Eqn 2.17):

$$T_l = T_o [e^{-\tau_c}(e^{-\tau_l} - 1)] + T_e \left[\frac{(b_m \tau_l^* + \tau_c)}{\tau_\nu} (1 - e^{-\tau_\nu}) - (1 - e^{-\tau_c}) \right] \quad (5.1)$$

plays an important role in the modelling. Simplifying **approximations** are made in the above equation to reduce the complexity of the problem. As mentioned in Chapter 2, the non-thermal field inside the cloud and in **front** of the cloud have been ignored in the above equation. From the discussion in the previous sections, it appears that the low-frequency carbon lines arise in the cold, neutral **gas**. Since the electron temperature of the cloud T_e is then expected to be ~ 100 K which is much less than the **background** radiation temperature, T_o , the second term can also be ignored in **Eqn 5.1**. Furthermore, at the low frequencies under consideration, which preferentially sample low-density ionized regions, the line and continuum optical depths are expected to be very small ($\tau_l \ll 1$ & $\tau_c \ll 1$). Hence the above equation reduces to the simple form:

$$\frac{T_l}{T_o} = -\tau_l \quad (5.2)$$

Thus the observed line-to-continuum ratio is equal to the line optical depth of the medium if both the line and continuum regions have the same **beam-covering** factors. This simplifies the analysis. At low frequencies, the line width is **expected** to be **affected** by pressure and radiation broadening and hence the correct physical quantity to use is the integrated optical depth. From **Eqn 5.2**,

$$\frac{\int T_l d\nu}{T_o} = - \int \tau_l d\nu \quad (5.3)$$

Note that the temperatures referred to in **Eqn 5.3** are brightness temperatures. In practise, the antenna temperature is recorded by radio telescopes. The antenna temperature (T_A) is related to the brightness temperature (T_B) through the beam dilution factor and the main beam efficiency η as follows:

$$T_A = \eta \frac{\Omega_S}{\Omega_B} T_B \quad (5.4)$$

for $\Omega_S < \Omega_B$. Here Ω_S is the solid angle subtended by the source whereas Ω_B is the beam solid angle.

$\frac{\Omega_S}{\Omega_B}$ is the **beam** dilution factor which at low **frequencies** *can* be **different** for line and continuum. If Ω_L is the solid angle subtended by the line region and Ω_C is that of the continuum background, then for $\Omega_L < \Omega_C$, the true optical depth of the line in terms of the observed antenna temperatures is given by

$$\tau_L = \frac{\Omega_C}{\Omega_L} \frac{T_{A,L}}{T_{A,C}} \quad (5.5)$$

If $\Omega_L \geq \Omega_C$ then the above equation reduces to $\tau_L = \frac{T_{A,L}}{T_{A,C}}$. At low radio frequencies, the continuum radiation in the Galactic plane is largely due to the non-thermal background and therefore it generally has a large effective beam filling factor. The angular extent of the line region thus plays an important role in determining the physical properties of the gas.

The true line optical depth τ_l is related to the LTE line optical depth through the departure coefficients, b_n and β_n as follows (as described in Chapter 2):

$$\tau_l = b_n \beta_n \tau_l^* \quad (5.6)$$

where from Shaver (1975), the LTE line optical depth is

$$\tau_l^* = 1.92 \times 10^3 \frac{EM}{\left(\frac{\Delta V_D}{c} \nu\right) T_e^{2.5}} Z^2 e^{X_n} \left[1 + 1.48 \frac{\Delta V_L}{\Delta V_D}\right]^{-1} \quad (5.7)$$

and

- EM = $\int N_e N_i dl$ is the line emission measure due to the recombining ion in pccm^{-6} .
- ΔV_D = Doppler full-width at half maximum.
- ΔV_L = Lorentzian full-width at half maximum.
- ν = Rest frequency of the recombination line.
- Z = Effective atomic charge.
- $X_n = \left(\frac{1.58 \times 10^5}{n^2 T_e}\right)$.

The integral of the line optical depth over the line width is obtained by integrating Eqn 5.6 after substituting for τ_l^* from Eqn 5.7:

$$\int \tau_l d\nu = 2.046 \times 10^6 T_e^{-5/2} e^{X_n} EM_l b_n \beta_n s^{-1} \quad (5.8)$$

Integral of Eqn 5.5 gives the measured optical depth and Eqn 5.8 gives the expected optical depth in terms of the physical properties of the line region. Modelling is done by a comparison of these two at various frequencies as a function of chosen parameters of the line region.

5.5.2 The Modelling Procedure

Each model is characterized by an electron temperature T_e , electron density n_e , emission measure EM, radiation temperature at 100 MHz T_{R100} and the carbon depletion factor δ_C . As discussed in Sec 5.3, the upper limits on T_{R100} , T_e and n_e are determined from the widths of the lines observed at 34.5 MHz. Further limits on T_{R100} can be obtained

from the continuum map at 34.5 MHz (**Dwarakanath** 1989) and also the "all-sky" map at 408 MHz by **Haslam** et. al. (1982). Once the parameter space is decided, the departure coefficients b_n and β_n which account for the non-LTE effects are determined using the computer code of Salem & Brocklehurst (1979) which assumes that the levels are in statistical equilibrium. The hydrogenic populations for carbon are generated by this method. However, carbon being a multi-electron system is expected to be influenced by the dielectronic-like process (Watson, Western & Christensen 1980, hereafter **WWC80**) involving the fine-structure levels in the ground state when the kinetic temperature of gas is comparable to 90 K which is the separation between the fine structure states. The departure coefficients of carbon, calculated under hydrogenic approximation and by including the effect of dielectronic-like processes are compared in the next Section. The beam dilution factor is applied to the observed line-to-continuum ratio using Eqn 5.5 to obtain the integrated line optical depth. From the integrated optical depth at one of the observed frequencies, the line emission measure is determined using **Eqn 5.8**. In the next step the expected **values** of the integrated optical depths are calculated for **different** n using the calculated emission measure and other parameters, and compared with other available observations. Further constraints, if any, such as pressure equilibrium with the ISM, are applied to narrow down the acceptable range of parameters.

Although the spatial resolutions and beam orientations at different frequencies **are** not the same (see Fig 5.4), which may have **resulted** in different clouds being sampled at different frequencies, we assume that the lines originate in clouds with similar physical properties. This is because the $l-v$ curves for all the three frequencies indicate that the line-forming gas lies between Galactocentric distances of 4.5 & 8 kpc and hence is likely to be the same. Moreover, very few low-frequency observations are available and it is almost impossible to obtain data with similar resolution at all these **frequencies**. Hence as a first approximation, we assume that all the **observed** lines arise in the same gas. However, it should be kept in mind that the different radial velocities at which the carbon lines at the three frequencies are observed do indicate **some non-overlap** in the emitting regions.

As discussed in **Sec 5.2**, our observations at 328 MHz indicate that the **line-emitting** region is likely to be 2° or larger in extent. Observation of **EMA95** at 76 MHz show that the carbon line regions in the inner Galaxy are likely to be $\sim 4^\circ$ in extent. Since the extent of the line-forming gas in the Galactic plane can even be larger than 4° , we explore models in which the line-forming region is ubiquitous (*i.e.* fills all the beams that are used) or 4° large or 2° in extent. In all the three cases, the **non-thermal** radiation is assumed to uniformly fill all the beams.

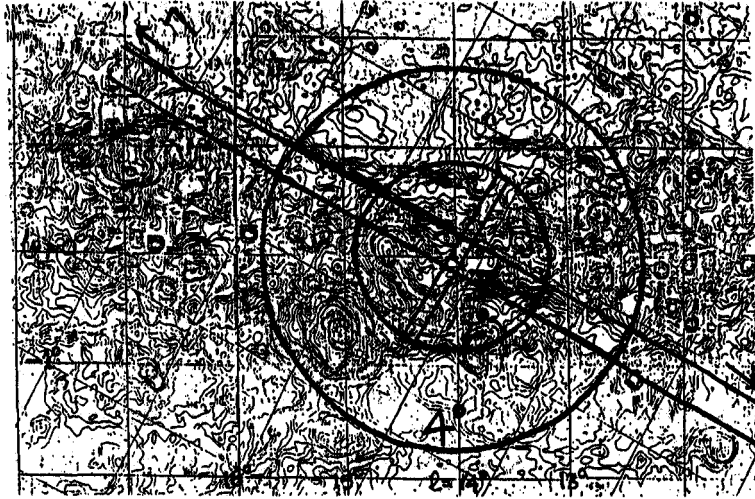


Figure 5.4 The brightness distribution towards the direction of Galactic longitude of 14° at 2.7 GHz (Reich *et.al.* 1990) in the Galactic plane is shown in this figure. The long rectangle represents the Gauribidanur beam ($21' \times 25^\circ$) used to observe carbon recombination lines at 34.5 MHz. Only a part of the beam ($\sim 7^\circ$) is shown along the declination direction. The small circle represents the ORT beam ($2^\circ \times 2''$) used at 327 MHz and the narrow rectangle shows the ORT beam ($2^\circ \times 6'$). The big circle indicates the $4^\circ \times 4^\circ$ Parkes beam used to observe carbon lines at 76 MHz (EMA95). All the beams are centred at the position $l = 14''$ and $b = 0^\circ$.

At all the frequencies, the ratio of the line temperature to the system temperature is taken to be equal to the line-to-continuum ratio. At low frequencies like 34.5 MHz and 76 MHz this is a reasonable assumption to make since the system temperature is dominated by the sky temperature. At 328 MHz, however, the brightness temperature of the non-thermal radiation field in the inner Galaxy is in the range 500 – 700 K whereas the receiver temperature is likely to be around 120 K which modifies the line-to-continuum ratio by a factor of ~ 1.2 . Owing to some problems in the calibration measurements using the ORT we did not obtain the line and continuum temperatures separately and have to use the ratio of line temperature to the system temperature obtained from the 1-bit correlator system. The error introduced by taking this to be the line-to-continuum ratio would be only 20 % and in most cases lies within the 1 σ error bar of the observed point.

5.5.3 Criteria for selecting Good Models

After generating the model optical depths as a function of frequency, we needed some criteria to select the ones which best explains the observations. In a majority of the positions, we have ≤ 3 observed data points on which to base the goodness of our

models. We used the **following** criteria in sequential order to **distinguish** the 'good' models from the 'bad' ones:

- *Visual inspection.* This was the main filter. Since in most of the cases we have only three observed data points, a χ^2 fit **was** inappropriate and we depended on the discerning abilities of our eyes.
- *Pathlengths predicted by the models.* **Since** the line widths at all the observed frequencies are similar, the width is most likely due to large-scale motions. If these motions are due to Galactic rotation then the clouds should be distributed over several kiloparsecs along the line-of-sight. Thus models which require small pathlengths can be ruled out.
- *Thermal pressure predicted by the model.* If the **gas** is associated with the cold neutral medium then it is reasonable to expect it to be in pressure equilibrium with the **ISM**. Thus only models which produce pressures in the range of **1000-9000 cm⁻³** would be acceptable. This criterion rules out some of the models allowed by the above two constraints.

5.5.4 Generating **the** Models

Any model that we generate needs to satisfy the observables: the integrated optical depth $\frac{\int T_1 d\nu}{T_{\text{sys}}}$ and the line width ΔV . The models should also be consistent with the upper limits on temperature T_e , density n_e and the radiation temperature T_{R100} which were obtained in **Sec 5.3**.

The radiation temperature in the inner Galaxy at **100 MHz**, extrapolated from the **34.5 MHz** continuum map (Dwarakanath 1989) and averaged over a typical **25°** stretch across the Galactic plane is ~ 5000 K. As noted in Table 5.3, the upper limit on T_{R100} from the line width < 5000 K. We assumed two model values for T_{R100} - **2500 K** and **1250 K** for calculating the departure coefficients. From Table 5.3, we see that the largest permissible electron density is $\sim 1.5 \text{ cm}^{-3}$. However, this assumes that the entire line width at **34.5 MHz** is due to collisional broadening which is obviously not true. For consistent modelling, we calculated the maximum allowed electron density for each direction from the line widths and the radiation temperature used in the model. We constructed models with electron densities ranging from **0.001 cm⁻³** to the upper limit calculated from line widths. The lower end for n_e was fixed by the maximum allowed pathlengths through the Galaxy. The **temperature** range of **20 - 400 K** was considered based on typical temperatures in molecular clouds, in **HI** clouds and in

C II regions observed at higher frequencies, all of which are prospective sites of origin of low frequency carbon lines.

Table 5.7 The integral of the line-to-continuum ratio over the line width observed at various frequencies. Dash indicates that no data for that frequency is available.

No.	Source	$\frac{T_{\text{line}} \nu}{T_{\text{sys}}} \text{ s}^{-1}$				
		n~686 25 MHz	n~575 34.5 MHz	n~539 42 MHz	n~443 76 MHz	n~271 328 MHz
1	G352+0	-	-2.6 ± 0.3	-	-3.8 ± 2.0	6.9 ± 0.7 (G355+00)
2	G00+00	-	-3.0 ± 0.5	-9.8 ± 3.8	-4.6 ± 1.5	13.6 ± 1.9
3	G05+00	-	-1.8 ± 0.2	-	-4.9 ± 2.4 (G06+00)	9.8 ± 0.6
4	G10+00	-	-3.5 ± 0.4	-	-5.1 ± 2.9	10.7 ± 1
5	G14+00	-	-4.0 ± 0.4	-	-5.6 ± 2.4	12.7 ± 4.1
6	G16.5+0	-	-2.3 ± 3.4	-	-9.8 ± 2.6	7.0 ± 0.6
7	G63+00	-	-2.2 ± 0.2	-	-	<3.7
8	G75+00	-1.6 ± 0.3	-1.5 ± 0.2	-	-	-
9	DR21	-3.7 ± 1.0	-1.6 ± 0.3	-	-	-

Column 3 - data from Konovalenko (1984) and Golykin & Konovalenko (1990).

Column 4 - our data.

Column 5 - data from Smirnov *et.al.* 1996.

Column 6 - data from EMA95.

Column 7 - our data.

Very little information on the depletion of carbon is available. The presence of grains in the ISM suggests that some fraction of carbon is depleted. We hence, assumed a depletion factor of 0.5 to start with and varied it from 0.1 to 0.9. The line-to-continuum ratios integrated over the line widths which are the primary constraints for the models are tabulated in Table 5.7.

The following three cases were considered for the angular extent of the line-emitting regions.

- **Case 1:** The thermal cloud and the non-thermal radiation cover the same region of the various beams used in this analysis and that there is no beam dilution at any of the frequencies *i.e.* $\frac{\Omega_L}{\Omega_C} = 1$ in Eqn 5.5 .
- **Case 2:** The line-producing cloud is 4° in extent and the non-thermal radiation fills all the beams. Hence at 34.5 MHz, the dilution factor is 0.19. There is no

dilution (*i.e.* $\frac{\Omega_L}{\Omega_C} = 1$) at 76 MHz and 328 MHz.

- **Case 3:** The thermal cloud is 2° in extent **and** the non-thermal radiation fills all the beams, Hence the dilution factors are 0.25 at 76 MHz and 0.09 at 34.5 MHz.

In summary, the parameter space that we used for modelling the low-frequency carbon recombination line-forming regions in the Galactic plane were:

electron density, n_e	0.001 to 0.5 cm^{-3}
electron temperature, T_e :	20 K to 400 K
radiation temperature, T_R :	1250 K & 2500 K
carbon depletion factor, δ_C :	0.1 to 0.9
cloud size	$2^\circ, 4^\circ, \geq 4''$.

(a depletion factor of **0** means that all the carbon is depleted onto grains whereas $\delta_C = 1$ means that all the carbon is in the gaseous form)

Hydrogenic & Dielectronic Models:

Prior to the introduction of the dielectronic-like recombination in carbon and its possible effect on the populations of high quantum states (**WWC80**, Walmsley & Watson 1982), it was believed that the level populations in carbon are essentially determined by hydrogenic processes. This is still considered true for low-temperature (~ 20 K) plasma in which very few electrons are sufficiently energetic to participate in the dielectronic-like processes. However, calculations show that, even at low temperature, significant differences are seen near large quantum numbers especially if the ratio of level populations of the fine structure states $^2P_{3/2}$ & $^2P_{1/2}$ is **subthermal** *i.e.* $R < 1$ (see Eqn 2.35). Subthermal populations of the fine structure levels occur at low electron densities. At higher electron densities, $R \sim 1$ and the dielectronic level populations approach the hydrogenic ones.

In Fig 5.5 (a), the variation of $b_n\beta_n$ with n is shown for both hydrogenic and dielectronic models for $T_e = 20$ K and $n_e = 0.3 \text{ cm}^{-3}$. Both the models predict similar variation in $b_n\beta_n$ with n for $n < 300$. However for larger n values ($n \geq 300$), the difference in the value of $b_n\beta_n$ for hydrogenic and dielectronic models are significantly different. For still lower electron densities, the difference between the two models increases as shown in Fig 5.5 (b) for $n_e = 0.05 \text{ cm}^{-3}$. For these physical parameters, $b_{600}\beta_{600} = 0.226$ in the hydrogenic case whereas $b_{600}\beta_{600} = 0.5316$ in the dielectronic case which is a change by a factor > 2 in the optical depth at $n = 600$! Since our results include the observations at $n=575$ where the two processes predict significantly

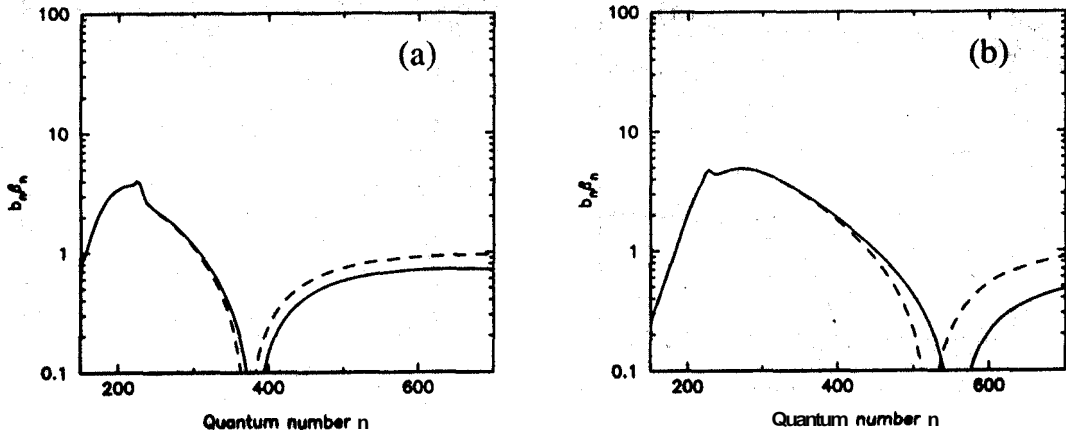


Figure 5.5 The variation in the product $b_n \beta_n$ with quantum number is shown in the figure for hydrogenic and dielectronic models at 20 K. In (a), $n_e = 0.3 \text{ cm}^{-3}$ whereas in (b), $n_e = 0.05 \text{ cm}^{-3}$. The variation in the function $b_n \beta_n$ for hydrogenic level populations is shown by the solid line and that for dielectronic level populations is shown by the dashed line. b_n and β_n are calculated using the Brocklehurst & Salem (1977) code modified by Walmsley & Watson (1982) and PAE94.

different level populations even for $T_e = 20 \text{ K}$ we use dielectronic models for both the low and high temperature cases. The computer code originally developed by Salem & Brocklehurst (1977) and later modified by Walmsley and Watson (1982) to include the **dielectronic-like** recombination and by **PAE94** to extend the calculations to $n = 10000$ was used to calculate the departure coefficients.

5.5.5 Effect of change in physical parameters on the product $b_n \beta_n$

In this section, the effect of change in T_{R100} , T_e , n_e and δ_C on the energy level populations is demonstrated. We have considered the combinations $T_e = 20 \text{ K}$ & $n_e = 0.3 \text{ cm}^{-3}$ and $T_e = 100 \text{ K}$ & $n_e = 0.007 \text{ cm}^{-3}$. These combinations are typical of the physical **parameters** of the molecular gas and the **CNM** respectively. T_{R100} is varied from 2500 K to 0 K to demonstrate the effect of radiation temperature on the level populations for the two combinations. Varying the depletion factor of carbon from 0.1 to 0.9 gives an idea of its effect on the level populations for the two combinations. In **Figs 5.6 to 5.9**, the **cusp** in the function $b_n \beta_n$ vs n indicates the turnover from emission to absorption lines with increasing n .

In Fig 5.6, change in the nature of $b_n \beta_n$ with change in T_{R100} is shown. Increase in T_{R100} has no effect on $n < 300$ and negligible effect on larger n values if $T_e = 20 \text{ K}$ and $n_e = 0.3 \text{ cm}^{-3}$ as shown in Fig 5.6 (a). This is because at this density, **collisional** processes dominate over radiative processes. However, this is not the case when

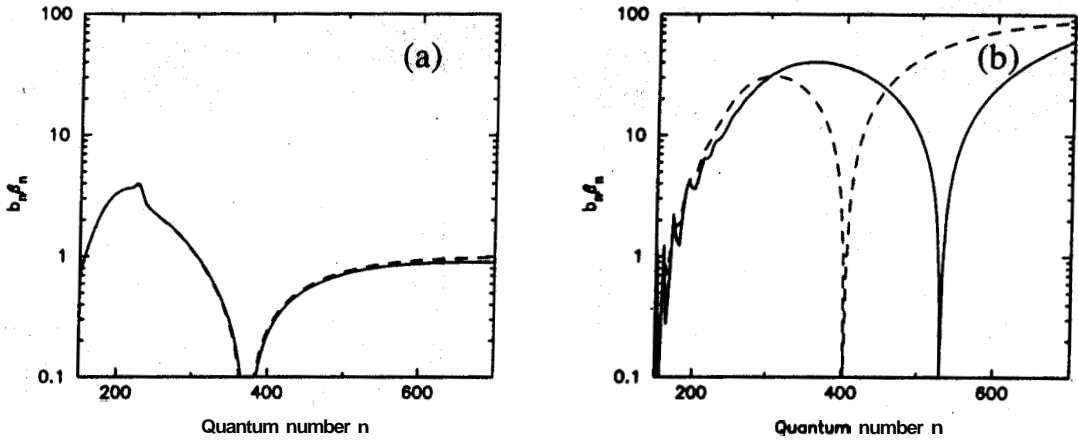


Figure 5.6 The variation in the nature of $b_n \beta_n$ with change in T_{R100} . In (a), $T_e = 20$ K & $n_e = 0.3 \text{ cm}^{-3}$. In (b), $T_e = 100$ K and $n_e = 0.007 \text{ cm}^{-3}$. The solid line is in the absence of a nonthermal background and the dashed line is for $T_{R100} = 2500$ K.

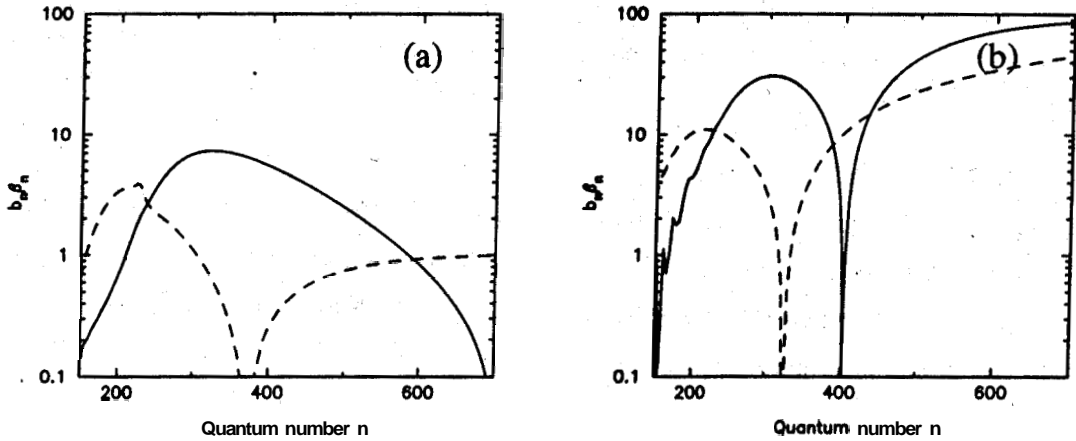


Figure 5.7 The effect of varying the electron density on the level populations is demonstrated for two temperatures in the figures here. The solid line is for $n_e = 0.007 \text{ cm}^{-3}$ and the dashed line is for $n_e = 0.3 \text{ cm}^{-3}$. In (a), $T_e = 20$ K whereas in (b), $T_e = 100$ K. $T_{R100} = 2500$ K for both the cases.

$n_e = 0.007 \text{ cm}^{-3}$ and $T_e = 100$ K shown in Fig 5.6 (b). In this combination, since n_e is small, T_{R100} influences the populations **significantly**. Thus, increase in T_{R100} acts equivalently to an increase in n_e which lowers the quantum number at which the **turnover** from emission to absorption occurs.

In Fig 5.7, the nature of $b_n \beta_n$ has been shown for two values of n_e at a given temperature. The significant effect on the populations while going from $n_e = 0.007 \text{ cm}^{-3}$ (solid line) to $n_e = 0.3 \text{ cm}^{-3}$ (dashed line) is clearly seen for $T_e = 20$ K (Fig 5.7 a) and for $T_e = 100$ K (Fig 5.7 b). In both the **cases**, the emission lines turnover into absorption at a lower quantum number as n_e is increased. In other words, increase in n_e speeds up the **thermalization** process so that relatively lower energy levels become

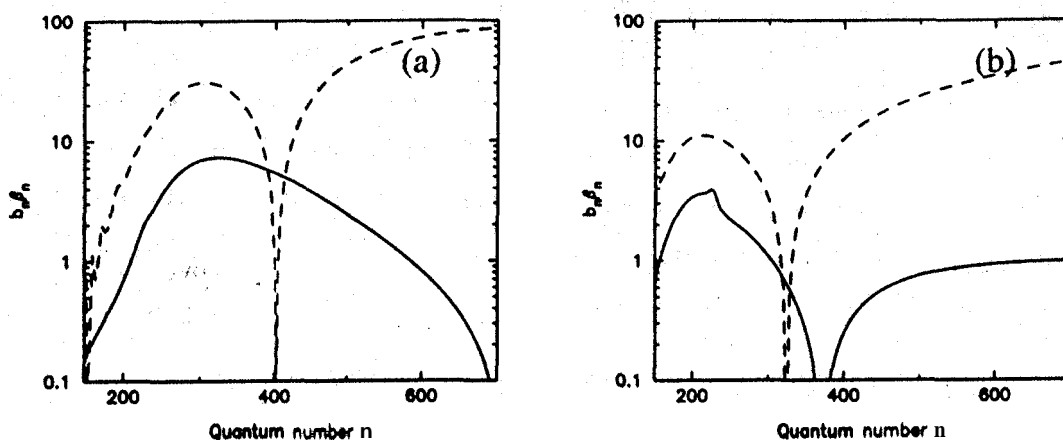


Figure 5.8 Effect of change in T_e on the the product $b_n \beta_n$. In both the figures, the solid line is for $T_e = 20$ K and the dashed line is for $T_e = 100$ K. In (a), $n_e = 0.007 \text{ cm}^{-3}$ and in (b), $n_e = 0.3 \text{ cm}^{-3}$. $T_{R100} = 2500$ K for both the cases.

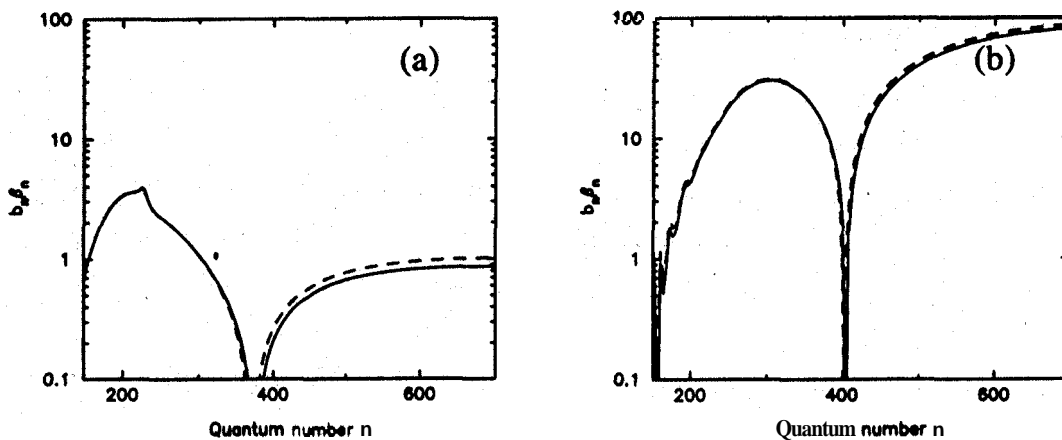


Figure 5.9 Variation in **level** populations due to change in depletion factor of carbon is shown here. In (a), $T_e = 20$ K and in (b), $T_e = 100$ K. The solid line shows the level populations for $\delta_C = 0.1$ and the dashed line is for $\delta_C = 0.9$. $T_{R100} = 2500$ K for both the cases.

thermalized. Moreover, increase in n_e also leads to thermalization of the fine-structure populations, hence decreasing the efficiency of dielectronic-like processes in populating **large- n** levels. The equivalent of b_n for the fine-structure states ($^2P_{3/2}$ and $^2P_{1/2}$) is the quantity R (see Eqn 2.35). Lower values of R are desirable for **dielectronic-like** recombination to be effective. For $n_e = 0.007 \text{ cm}^{-3}$, $R = 0.01$ whereas for $n_e = 0.3 \text{ cm}^{-3}$, $R = 0.3$.

In Fig 5.8, how a change in T_e influences the level populations has been demonstrated. For both the densities, dielectronic-like recombination enhances the amplification factor $b_n \beta_n$ as T_e increases. This is clearly because as T_e increases, the number of electrons which are sufficiently energetic to excite **the fine-** structure increases. These

electrons are capable of recombining dielectronically and enhancing the level populations at high quantum numbers.

Lastly, in Fig 5.9, we show the effect of changing the depletion factor of carbon for the two combinations of T_e and n_e . In (a), $T_e = 20$ K, $n_e = 0.3 \text{ cm}^{-3}$ whereas in (b), $T_e = 100$ K, $n_e = 0.007 \text{ cm}^{-3}$. The depletion factor is varied from 0.1 to 0.9. This change seems to have negligible influence on the level populations as is evident from the figure even though the value of R changes from 0.05 to 0.006 for $n_e = 0.007 \text{ cm}^{-3}$ and from 0.7 to 0.25 for $n_e = 0.3 \text{ cm}^{-3}$ on going from $\delta_C = 0.1$ to 0.9.

5.5.6 Results of Modelling - Positions in the Inner Galaxy

In the previous section, we described the effect of various physical parameters on the level populations. In this section we construct models which fit the observed data using these level populations.

Low-Temperature ($T_e = 20$ K) Models:

Here we investigate the range of electron density n_e which fit the observed data for $T_e = 20$ K. This low temperature is typical of molecular clouds in the ISM and hence these models indirectly assume that the ionized carbon is coexistent with the molecular gas. Furthermore, since molecular clouds are not necessarily in pressure equilibrium with the ISM (giant molecular clouds are self-gravitating), no constraints on the thermal pressure of the gas is imposed.

Within the range of n_e defined by the line width at 34.5 MHz, models with $T_e = 20$ K were constructed with $T_{R100} = 2500$ K & 1250 K for 3 cloud sizes of 25° , $4''$ and $2''$. We could find no models for cloud sizes of $4''$ or $2''$ (Cases 2 & 3) that could fit the observed optical depths at low frequencies as well as the frequency of turnover from emission to absorption. Fig 5.10 shows the dielectronic models with $T_e = 20$ K and $n_e \sim 0.2 - 0.4 \text{ cm}^{-3}$ which seem to fit the integrated optical depths at 328 MHz & 76 MHz for various positions observed in the inner Galaxy if the cloud size is $> 4^\circ$ (i.e. Case 1). As seen in the figure, all the models predict the observed behaviour; emission lines at high-frequencies and absorption lines at low frequencies. However, we could not find models which also fitted the 34.5 MHz data point when the beam dilution is assumed to be = 1 i.e. cloud sizes are $\geq 25^\circ$. The models indicate that the sizes of the line-forming clouds are between 4° and 25° . Using the observed value at 34.5 MHz and the model prediction, the angular size of the cloud is obtained and listed in Table 5.8. We also found models with lower n_e which explain the $n = 272$ and $n = 575$ points but not the $n = 443$ point. But, since no parameter could be adjusted to explain the

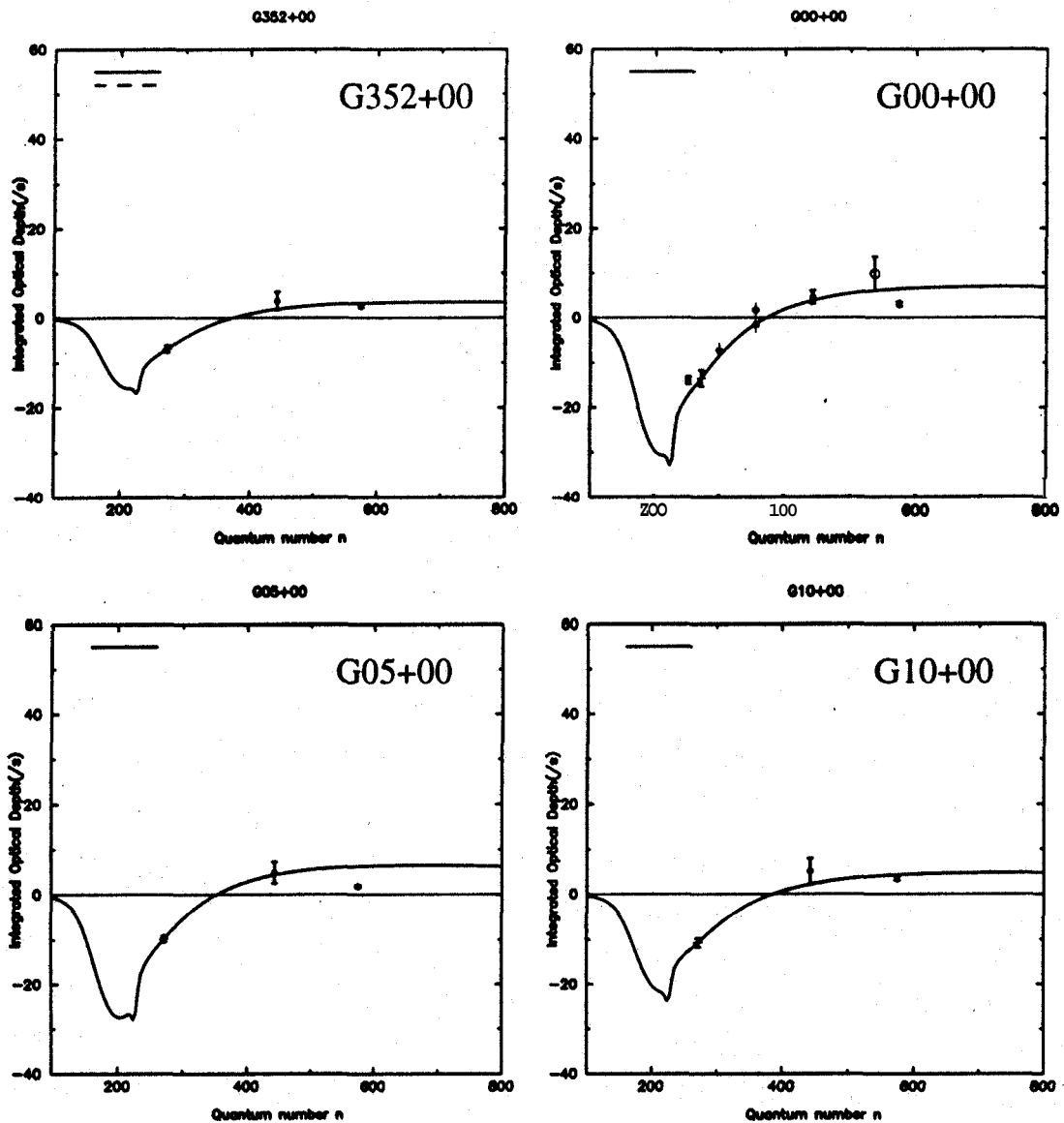


Figure 5.10 Oielectronic Models for G352+00, G00+00, G05+00, and G10+00 are shown in the figure for $T_e = 20\text{ K}$. The star represents the observed data point near $n = 575$, dot is the point near $n = 443$ and the cross is the data point observed near $n = 271$. The solid line represents the model fit for $T_{R100} = 1250\text{ K}$ and the dashed line is the fit for $T_{R100} = 2500\text{ K}$. n_e for G352+00 is 0.3 cm^{-3} , for G00+00 is 0.3 , for G05+00 is 0.4 and for G10+00 is 0.25 cm^{-3} . Towards the Galactic centre, the $n = 252$ & 300 points are from Pedlar *et.al.* (1978), $n = 356$ from Anantharamaiah *et.al.* (1990) and $n = 538$ is from Smirnov *et.al.* (1996).

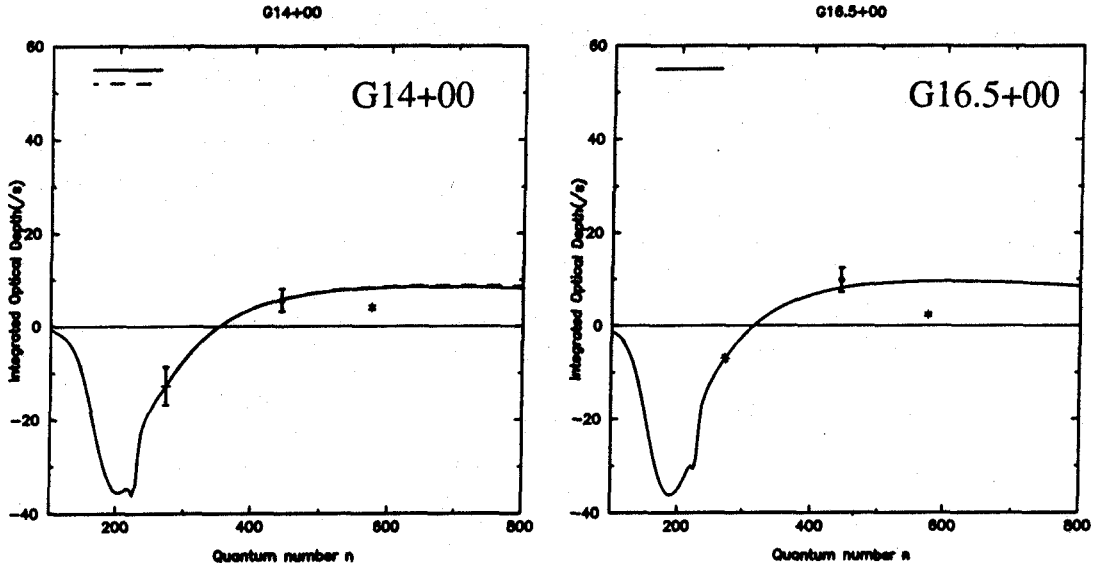


Figure 5.10 (contd) Dielectronic Models for G14+00 and G16.5+00 for $T_e = 20$ K. The points and curves are coded as described in the caption of the first part of this figure. n_e for G14+00 is 0.4 cm^{-3} for both T_{R100} whereas for G16.5+00 is 0.7 cm^{-3} and $T_{R100} = 1250$ K.

76 MHz point, we rule out those models. Models with $T_e = 20$ K for cloud sizes of 4° or 2° (Cases 2 & 3) failed to reproduce the large optical depths at low frequencies that these cloud sizes require.

The fitted physical parameters of the models shown in Figs 5.10 are listed in Table 5.8 for two assumed radiation temperatures, $T_{R100} = 2500$ K and 1250 K. In column 6, the emission measure calculated from the $n = 272$ point is tabulated. It varies from 0.003 to 0.009 pc cm^{-6} . In the next column, the pathlength through the cloud required by the model is listed. These range from 0.02 to 0.07 pc, indicating sheet-like geometry for the line-forming region. Column 8 shows the thermal pressure in the cloud for the particular combination of T_e and n_e assuming $\delta_C = 0.5$. Since the gas with this temperature is presumed to be associated with molecular gas, the cloud need not be in thermal equilibrium with the ISM. The last column shows the angular size of the cloud implied by the difference between the observed and model optical depths at 34.5 MHz. The cloud size ranges from 5° to 20° for the different positions, The models are insensitive to change in the radiation temperature. This is because collisions in the electrons dominates over radiative processes in determining the level populations. In some of the cases, we were unable to find a model for $T_{R100} = 2500$ K because the deduced physical parameters predicted line widths which exceeded the observed values at 34.5 MHz.

Table 5.8 Physical properties of the **partially** ionized gas from model fits to the observed carbon recombination lines at 34.5 MHz, 75 MHz and 328 MHz for $T_e = 20$ K.

$T_{R,100}$ K	No.	Position	Case 1 : No Beam Dilution					θ_{Cloud} (NS)
			T_e K	n_e cm^{-3}	EM $\times 10^{-3}$ pc cm^{-6}	S pc	$n_{\text{H}} T_e$ $\times 10^4$ $\text{cm}^{-3} \text{K}$	
2500	1	G352+00	20	0.3	3.2	0.04	4.0	20°
	2	G00+00	20	-	-	-	-	-
	3	G05+00	20	-	-	-	-	-
	4	G10+00	20	0.25	4.2	0.07	3.3	20°
	5	G14+00	20	0.4	7.8	0.05	5.3	12.5°
	6	G16.5+0	20	-	-	-	-	-
≤ 1250	1	G352+00	20	0.3	3.2	0.04	4.0	20°
	2	G00+00	20	0.3	6.2	0.07	4.0	12.5"
	3	G05+00	20	0.4	6.0	0.04	5.3	7.5"
	4	G10+00	20	0.25	4.2	0.07	3.3	20°
	5	G14+00	20	0.4	7.8	0.05	5.3	12.5°
	6	G16.5+00	20	0.7	9.1	0.02	9.3	5"

Column 6 lists the emission measure calculated from the observed point near 328 MHz.

Column 7 lists the pathlengths predicted by the models.

Column 8 lists the pressure in the gas in terms of $n_{\text{H}} T_e$.

Column 9 lists the angular size of the line-forming cloud as found from the 34.5 MHz observation.

A '-' (dash) as an entry indicates that we **were** unable to find a model which explained the observed optical depth at 76 MHz and 328 MHz and the width at 34.5 MHz. Number abundance of carbon is assumed to be $n_{\text{C}}/n_{\text{H}} = 3 \times 10^{-4}$ times and the depletion factor of carbon is assumed to be 0.5. The Gauribidanur E+W total power beam is 21' x **25°**.

As seen in Fig 5.10, the low **temperature** models predict strong lines near $n \sim 200$. Observations near 800 **MHz** in the Galactic plane are required to test these predictions. Existing observations near $n \sim 166$ (**Lockman** 1976, Heiles *et.al.* 1996) are **not** sensitive enough to obtain any constraints. Similar predictions by the low temperature models towards **Cas A** have not **been** confirmed (**see** Chapter 4 & **PAE94**).

Although these models explain the observed optical depths with n_e and T_{R100} within the limits defined by the line width at 34.5 **MHz**, the main objection to them comes from the extremely short pathlengths and very large angular extents that they predict (columns 7 & 9 of Table 5.8). Pathlengths of ~ 0.05 pc indicate that the lines probably originate in a thin layer of ionized carbon on the surface of large and nearby molecular

clouds, ionized by the ambient ultraviolet radiation. On the other hand, the large widths of the lines which may be due to Galactic rotation, requires the gas to be distributed between 4 kpc and 7.5 kpc as shown in Fig 5.2. Hence it appears that models which predict longer pathlengths are required. Moreover, pressure and radiation broadening due to such low-temperature plasma with $n_e \sim 0.3 \text{ cm}^{-3}$ and the $T_{R100} \sim 2500 \text{ K}$ or 1250 K can account for a substantial part of the line width at 34.5 MHz. This does not agree with the **conclusion**, based on the nearly similar extents of the lines at the three frequencies, that the line widths are a result of large-scale motions. The 'good' models should, thus, have a small contribution to the line width from pressure and radiation broadening. We investigated the **effect** of a change in the depletion factor δ_C on the models and found no significant **effect** and the physical parameters of the model remained unchanged as noted in the previous section. We now turn to high-temperature models to explain the observed **low- ν** recombination lines of carbon.

High-Temperature ($T_e > 30 \text{ K}$) Models

In this section, we model the carbon line-forming regions assuming temperatures which are typical of neutral HI clouds (i.e. $30 \text{ K} < T_s < 400 \text{ K}$). Since HI clouds are expected to be in pressure equilibrium with the ISM, we require that thermal pressures (P/k where $P = nkT$ is the gas equation) predicted by the models **fall in** the range from 1000 to $9000 \text{ cm}^{-3} \text{ K}$ (Jenkins *et al.* 1983). This constraint considerably reduces the number of acceptable models. As mentioned before, dielectronic-like process is most efficient in gas with temperature close to 100 K and low electron densities. These conditions are conducive to maintaining a sub-thermal population of the fine-structure levels ($^2P_{3/2} - ^2P_{1/2}$) which in turn enhances the dielectronic-like processes in carbon (**WWC80**). Hence in the plasma under consideration here, dielectronic-like recombination should have **significant** effect on the level populations.

Models were constructed for two different values of the background radiation temperature, $T_{R100} = 2500 \text{ K}$ & 1250 K . At each of these two values of T_{R100} , three cloud sizes mentioned earlier (i.e. 2° , 4° , $\gg 4''$) were considered. The emission measure was determined by the observed integrated optical depth at 328 MHz. We found no models that could fit the observations when the cloud size is very large i.e. the **beam** dilution factor at 34.5 MHz is ~ 1 . This is a significant result in that it seems to indicate that the observations at low frequencies are limited by beam dilution effects. Of the six positions for which models were tried, no satisfactory fit could be obtained for two positions i.e. **G05+00** and **G16.5+00**. The results of the fits for the other 4 positions are shown in Fig 5.11 and tabulated in Table 5.9.

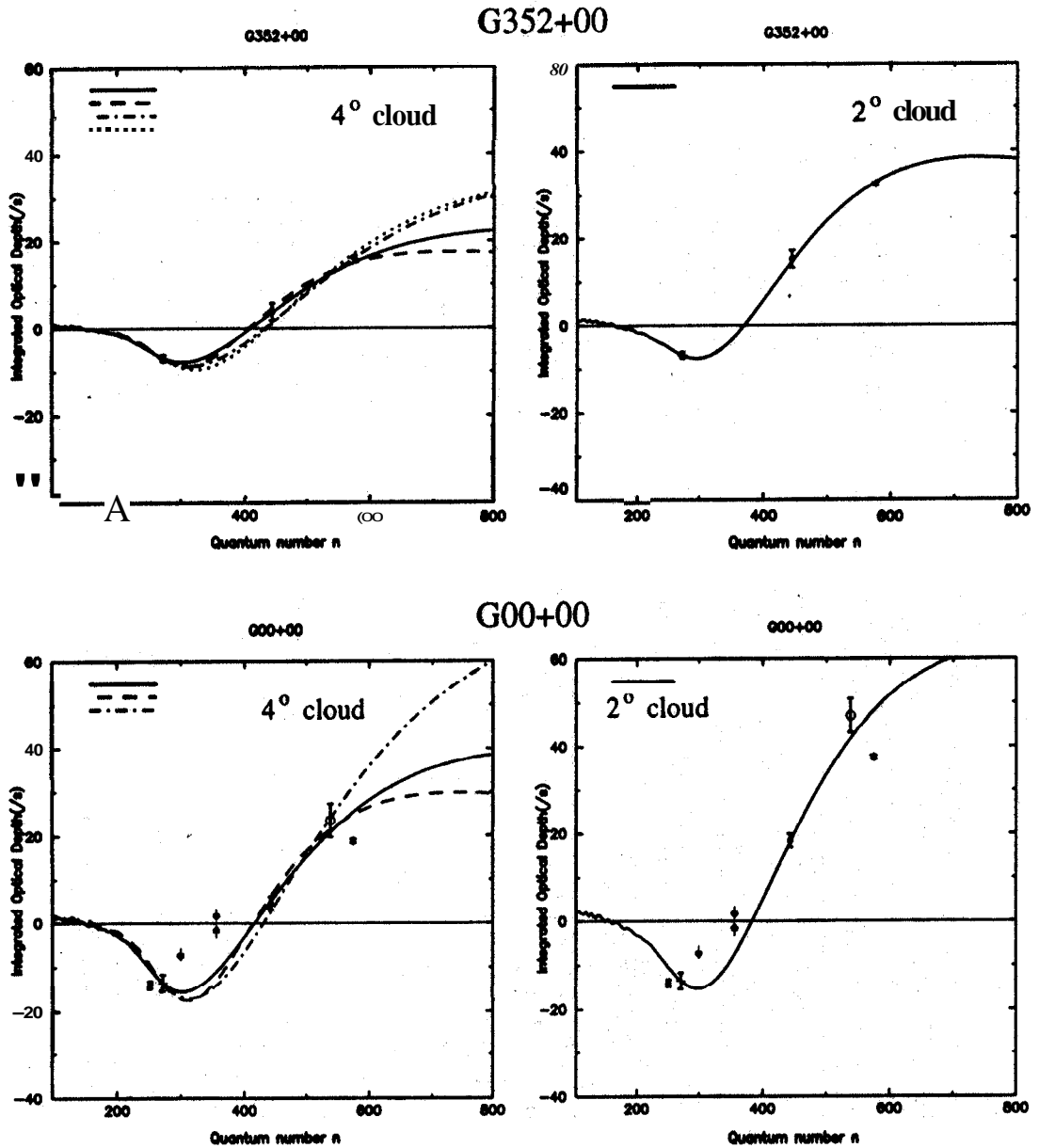


Figure 5.11 High- T_e Dielectronic models which explain the observed carbon recombination lines at low frequencies are shown for G352+00 and G00+00. The models plotted here are listed in Table 5.9.

Table 5.9 High- T_e models. Physical properties of the ionized carbon gas from the recombination line observations at 34.5 MHz, 75 MHz and 328 MHz.

$T_{R,100}$	No.	Position	Results of Dielectronic Models:									
			Case 1 : 4° Cloud					Case 2 : 2° Cloud				
			T_e	n_e	EM	S	$n_H T_e$	T_e	n_e	EM	S	$n_H T_e$
K	cm^{-3}	$\times 10^{-3}$ pccm $^{-6}$	pc	cm^{-3}K	K	cm^{-3}	$\times 10^{-3}$ pccm $^{-6}$	pc	cm^{-3}K			
2500	1	G352+00	90	0.01-0.003	10.6-11.3	106-1255	6000-1800	250	0.005	49.6	1984	8333
	2	G00+00	80	0.01-0.003	17.5-18.6	175-2067	5333-1600	150	0.007	45.2	918	7000
	3	G05+00	-	-	-	-	-	-	-	-	-	-
	4	G10+00	85	0.007-0.003	15.3-16.1	312-1789	3967-1700	180-190	0.007-0.005	47.1-51.0	961-2040	8400-6333
	5	G14+00	80	0.01	16.5	165	5333	175	0.007-0.005	53.6	1094-2144	8167-5833
	6	G16.5+0	-	-	-	-	-	-	-	-	-	-
1250	1	G352+00	100	0.01-0.007	13-13.5	130-276	6667-4667	-	-	-	-	-
	2	G00+00	-	-	-	-	-	-	-	-	-	-
	3	G05+00	-	-	-	-	-	-	-	-	-	-
	4	G10+00	95	0.015	18.5	82	9500	175-200	0.007-0.005	47.4-58.4	967-2336	8167-6667
	5	G14+00	95	0.015	22	97.8	9500	200	0.007	68.9	1406	9333
	6	G16.5+00	-	-	-	-	-	-	-	-	-	-

Level Populations include dielectronic-like processes. a '-' (dash) as an entry indicates that we were unable to find a model which explained all the three observations. The number abundance of carbon is assumed to be 3×10^{-4} times that of hydrogen and the depletion factor of carbon is assumed to be 0.5.

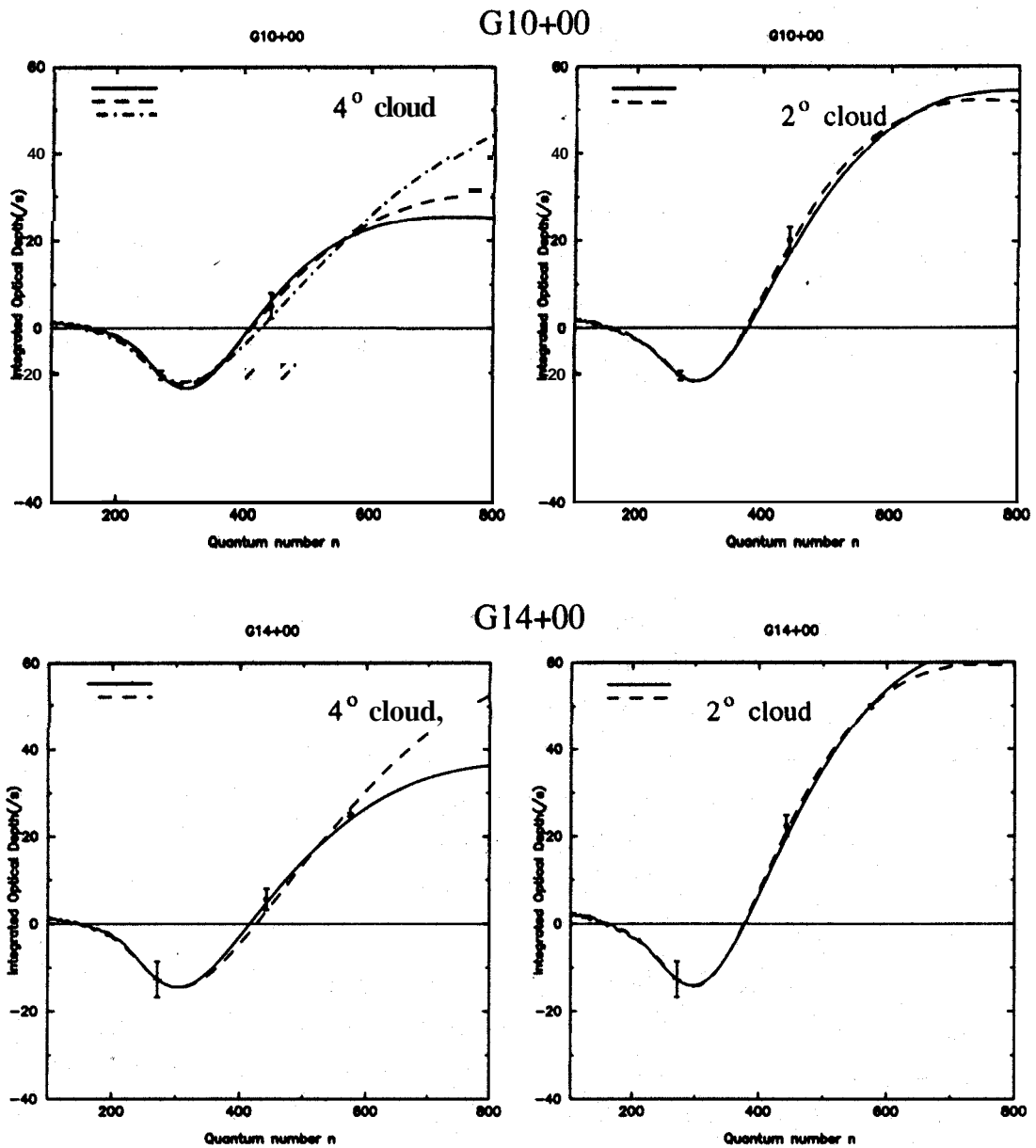


Figure 5.11 (contd) High- T_e Dielectronic models for G10+00 and G14+00. The models plotted here are listed in Table 5.9.

The models are constrained by the emission measure determined from the $n = 272$ data point. As shown in the Figs, all the models predict the general trend of variation in the optical depth with frequency - emission lines at high frequencies (*i.e.* $n < 350$) turnover into absorption lines at lower frequencies (*i.e.* $n > 450$). The turnover from emission to absorption occurs near $n \sim 415$ for the 4° cloud and around $n \sim 400$ for the 2° cloud. While the models with $T_{R100} = 2500$ K give good fit to the data at four of the positions, we were able to obtain models for only three of these directions if $T_{R100} = 1250$ K. Summarizing the results in Table 5.9, it appears that for a cloud, which is 2° in extent, the electron density is constrained to lie between $0.005 - 0.007 \text{ cm}^{-3}$ and the temperature in the range $150 - 250$ K for both the values of T_{R100} . These models require pathlengths of $1 - 2$ kpc through the line-forming region. On the other hand, if the cloud is assumed to be 4° in extent, then for $T_{R100} = 2500$ K, the cloud temperature is well-constrained between 80 K to 90 K whereas the electron density lies between $0.003 - 0.01 \text{ cm}^{-3}$. Pathlengths through the line-forming gas are between 0.1 to 2 kpc. For the same cloud size, models with electron temperature between 95 K and 100 K and electron density between 0.007 to 0.015 cm^{-3} give good fits for a reduced radiation temperature of $T_{R100} = 1250$ K. The required pathlengths through the line-forming gas are between 80 to 300 pc. Many visually-acceptable models were ruled out by the constraints listed in Sec 5.5.3. Densities lower than 0.003 cm^{-3} required extremely pathlengths (~ 50 kpc), whereas for $n, > 0.01$ large thermal pressures are unacceptable. ($> 10000 \text{ cm}^{-3} \text{ K}$). Change in the depletion factor of carbon had insignificant effect on the model predictions. The pressure in the selected models range from $1400-9500 \text{ cm}^{-3} \text{ K}$. According to Jenkins *et.al.*, most of the atomic hydrogen gas (50 %) has pressure between 2500 to $6500 \text{ cm}^{-3} \text{ K}$. About 33 % has pressure below $1000 \text{ cm}^{-3} \text{ K}$ and only 6 % of the gas has pressure above $10000 \text{ cm}^{-3} \text{ K}$ (Jenkins *et.al.* 1983).

In all these low- n , models, the change in the radiation temperature from 2500 K to 1250 K has a significant effect on the model predictions as is obvious from the physical parameters of the models listed in Table 5.9. At the low electron densities of all these models, the radiation temperature plays an important role in the determination of departure coefficients in addition to broadening the lines near 34.5 MHz.

Galactic Centre: Since the direction of the Galactic centre has been studied extensively in carbon lines as compared to other inner Galactic positions, we present the results in a separate section here. The best-fitting models to the line data towards Galactic centre are shown in Fig 5.11. Both the 4° - & 2° - models predict peak emission at

frequencies near 250 MHz ($n \sim 300$). At this frequency, the model predicts integrated line-to-continuum ratio of $\sim 15 \text{ s}^{-1}$. This ratio translates to a peak line strength of $\sim 2.5 \text{ K}$ if the continuum temperature is 3000 K and the line width is assumed to be $\sim 20 \text{ kms}^{-1}$. Pedlar *et.al.* (1978) have probed this direction at 242 MHz. Although a feature seems to be present near the expected line frequency ($\leq 1.4 \text{ K}$), it is weaker than that predicted by our models. Anish Roshi & Anantharamaiah (1996) have modelled the carbon line-producing gas assuming it to be 2° in extent with all the available data except the 34.5 MHz and 42 MHz data. For a $T_{R100} = 10^4 \text{ K}$, they find models with $T_e \sim 70 - 80 \text{ K}$, $n_e \sim 0.005 - 0.01 \text{ cm}^{-3}$ and pathlengths of $\sim 200 - 500 \text{ pc}$ which fit all the points except the limit at $n = 300$. However our models with a lower value of T_{R100} (which is based on the observed width of the 34.5 MHz), fails to explain the data at 34.5 MHz, 145 MHz and at 408 MHz. In short, the high- T_e models which are required to be in pressure equilibrium with the HI gas fit only the $n = 272$ and $n = 443$ points for both the cloud sizes in our modelling. For the 4° cloud, it also fits the 42 MHz point. However, it should be noted that this last data point from Smirnov *et.al.* (1995) may have a large error on the line width (Smirnov, private communication). The physical parameters of the models that Anish Roshi & Anantharamaiah (1996) obtained were $T_e = 70 - 80 \text{ K}$ and $n_e = 0.005 - 0.01 \text{ cm}^{-3}$ whereas Pedlar *et.al.* (1978) had found low-T, models with $n_e = 0.5 - 1 \text{ cm}^{-3}$ which fitted their observations. We find good visually-acceptable models with $T_e = 20 \text{ K}$ and $n_e = 0.3 \text{ cm}^{-3}$ as shown in Fig 5.10. The beam dilution predicted by this model for the optical depth at 34.5 MHz implies an angular size of $\sim 125'$ for the line-forming cloud if $T_{R100} \leq 1250 \text{ K}$. However the small pathlengths makes it difficult to explain the line widths. On the other hand, the high- T_e models that we obtain with $T_e = 80 \text{ K}$, $n_e = 0.003 - 0.01 \text{ cm}^{-3}$ for a 4° cloud and $T_e = 150 \text{ K}$, $n_e = 0.007 \text{ cm}^{-3}$ for a 2° cloud, fail to explain all the observed points. These models, however, give reasonable pathlengths of $0.2 - 2 \text{ kpc}$ through the line-forming gas and appear to be more plausible. The inability of these models to explain the observed optical depths may be due to the incorrect estimate of the size of the line-forming region. It appears necessary to observe near 242 MHz and 34.5 MHz with relatively high angular resolution to further constrain the physical properties of the partially ionized gas in this and other directions in the Galactic plane.

5.5.7 Other Galactic positions

Carbon lines at 34.5 MHz have been detected in absorption towards G63+00, G75+00 and DR 21. No recombination lines in emission were detected from G63+00 and G75+00 at 328 MHz. Absorption lines from the directions of G75+00 and DR 21

have been detected at 25 MHz by Konovalenko (1984) and Golyntin & Konovalenko (1990). However, since these two frequencies are nearby and both the lines are in absorption, it is difficult to constrain the model parameters. If an emission line is detected from these directions at higher frequencies ($\nu \sim 300$ MHz), then the turnover frequency can give meaningful constraints derived for the physical properties of the line-forming regions. Narrow ($\sim 4 \text{ kms}^{-1}$) **C158 α** and **C166 α** lines have been observed from DR 21 by Pankonin *et.al.* (1977a). However, these narrow lines are believed to originate in the warmer C II regions associated with the **H II** region in this direction and hence cannot be used in modelling the low-frequency line-forming regions. We, therefore do not discuss model fits to the observed data for these three positions. It may be useful to mention that large HI optical depth and ^{12}CO emission have been observed towards **G75+00** near 0 kms^{-1} , supporting the theory of origin of these **lines** in neutral gas. However, the case towards **G63+00** is somewhat **different**. The recombination line near 34.5 MHz appears at a velocity which is different from that of the deepest HI feature. It is, however, close to one of the peaks observed in ^{12}CO . Since the gas lying in the Galactic plane within longitude $< 17^\circ$ seems to possess fairly uniform physical properties, it is probable that the gas in the outer Galaxy is also of similar nature.

5.5.8 Discussion on the Probable Models of the Line-Forming Regions

If the partially ionized clouds in the inner Galaxy are assumed to be of similar angular sizes, then our modelling described in the previous sections shows that **all** the positions within $l = 352^\circ$ to $l = 17^\circ$ possess remarkably similar physical properties. If the cloud is assumed to be $\geq 4''$ in extent, $T_{R100} \leq 1250 \text{ K}$ and $T_e = 20 \text{ K}$, then the electron density seems to be $\sim 0.3 \text{ cm}^{-3}$ for most of the directions and the **pathlengths** are small ($< .1 \text{ pc}$). On the other hand, if the cloud is 4° or 2° large, then warmer models successfully fit the data. Model clouds with temperature between $80 - 100 \text{ K}$ and $n_e \sim 0.003 - 0.01 \text{ cm}^{-3}$ for both $T_{R100} = 2500 \text{ K}$ and 1250 K fit some of the data well for a 4° cloud whereas $T_e = 175 - 250 \text{ K}$ and $n_e = 0.005 - 0.007 \text{ cm}^{-3}$ fit the data well if the cloud size is assumed to be $2''$. In these models, the **pathlengths** are in the range $0.1 - 2 \text{ kpc}$. Thus, it is possible that the observed carbon recombination lines arise in clouds possessing a range of temperatures, electron densities and **angular** sizes. In this Section, the plausibility of the models described in the previous sections is discussed.

The low temperature ($T_e = 20 \text{ K}$) models give a good fit to the observed line strengths at 328 MHz and 76 MHz and by adjusting the beam dilution factor, the data can also fit the data at 34.5 MHz. However, these models are not favoured because of the extremely short pathlengths through the ionized gas predicted by them.

Since **the** widths of **the** lines detected at frequencies differing by a **factor** of ~ 10 , arc found to be very similar, it **implies that** pressure and radiation broadening, which are strong functions of frequency **cannot** be responsible for the **line** widths even at the low frequencies (*i.e.* ~ 34.5 **MHz**). The widths of the lines detected from the Galactic plane are, therefore, most likely due to differential Galactic rotation. Since this **requires** contribution from gas distributed between Galactocentric distances of 4 kpc and **7.5** kpc, the total pathlength predicted by our models should at least be a reasonable fraction of a kpc. **Instead**, all the low-temperature models gave pathlengths of only a fraction of a parsec (~ 0.02 **pc**). If this pathlength is to be divided into **smaller** regions and distributed over ~ 3 kpc, then it would require individual clouds to be ~ 0.008 pc thick which implies **an** extremely thin sheet-like geometry since the angular extent of the cloud are $5^\circ - 20^\circ$. The structure suggests that carbon in a **thin** outer layer of molecular clouds is photo-ionized by the ambient ultraviolet radiation field. This is **not** entirely improbable since the ionization fronts near star-forming **regions** are seen to have thickness ~ 0.02 pc. Nevertheless, it seems a contrived situation to expect many such thin layers distributed along a line-of-sight to mimic a region of $\sim 10^\circ$ in extent & **0.02** pc in **thickness**. It may be useful to recall that towards Cas A, the **low- T_e** models failed to explain the observed variation in optical depth with n and hence could straightaway be ruled out. But in the case of the Galactic plane positions, the low temperature models cannot be completely ruled out from the same argument because very few data points are available and also beam dilution effects are critical. One advantage of the low-temperature models is that the constraint on pressure equilibrium with the ISM is lifted since they assume coexistence with molecular gas. Since the carbon lines seem to be widely detectable in the inner Galaxy, it also seems to favour association with molecular gas which has maximum surface brightness in that region. Thus, the main criticism of the low temperature models is that the pathlengths required by **them** are extremely small and the angular extents are very large and **these** arguments are inconsistent with the observed widths.

The high temperature ($T_e > 30$ K) models which indirectly assume coexistence of ionized carbon with HI gas in the Galaxy successfully fit the observed data towards a few of the inner Galaxy positions if the angular size of the clouds were 4° or 2° . Large angular size of ($\sim 25^\circ$) the clouds was ruled out by these models. Due to the low electron densities (~ 0.007 cm^{-3}) of these **models**, the radiation temperature **has** considerable effect on the models **as** discussed in Sec 5.5.5. **The** number of positions that could be fitted with these models reduced **when** T_{R100} **was** decreased. For $T_{R100} = 5500$ **K** (such high radiation temperatures are ruled out by the observed line widths near **34.5 MHz**),

data from all the positions could be fitted assuming a cloud size of 2° or 4° , whereas for $T_{R100} = 1250$ K, only about half the positions had a 'good' model associated with them. Since radiation broadening near 34.5 MHz is expected to be a small fraction of the line width, $T_{R100} \leq 1250$ K seems to be more probable as it translates to a width of only ≤ 6 km s $^{-1}$ at 34.5 MHz. Failure to find acceptable models for all the positions with $T_{R100} = 1250$ K can be interpreted as being due to different cloud sizes. If the model was constrained to pass through the 328 MHz and 76 MHz observations in all such discrepant cases (G00+00, G05+00, G16.5+00), then the result suggests that the cloud size is larger than 2° for all these positions. Unfortunately, since we have data at only three frequencies, observed with different angular resolutions, we cannot obtain a more quantitative interpretation of this result. As mentioned before, the range of physical conditions in the clouds predicted by the warm models appears to be well-constrained. Due to the constraints placed by acceptable thermal pressures and pathlengths, the electron densities that satisfy the observed parameters lie in the range of 0.003 to 0.01 cm $^{-3}$. If the cloud has an angular size of 4° then the fitted temperatures are in the range 80 – 100 K whereas if the cloud is 2° in extent then the likely temperatures are between 175 K and 250 K. Although we could not find a warm-gas model for all the inner Galaxy positions, the positions for which we could obtain satisfactory models, predicted reasonable pathlengths for the line-forming clouds. Comparing this result with that towards Cas A, it appears likely that a significant fraction of low-frequency carbon recombination lines arise in warm gas associated with atomic HI. However, the electron densities in the atomic gas in the Perseus arm towards Cas A appear to be more than that in the inner Galaxy.

The range of physical parameters that we obtain in this analysis seems to favour an association with the partially ionized gas in the photo-dissociation regions (PDR) - especially the range of electron temperatures. A PDR, as defined by Tielens & Hollenbach (1985) are "regions where FUV radiation (6 – 13.6 eV) dominates the heating and/or some important aspect of the chemistry" and contains most of the atomic and molecular gas in the Galaxy. The low-excitation PDR discussed by HTT91 are illuminated by the interstellar radiation field (ISRF). These regions according to them include a warm ($T \geq 100$ K) atomic region comprised of hydrogen, oxygen and ionized carbon near the surface. Beyond that, is a cool ($T \sim 50$ K) partially dissociated region and still further in the interior is a cooler ($T \sim 10 - 20$ K) region. The PDRs encompass a wide range of physical properties. It is probable that carbon recombination lines arise at various depths in the PDR. From the present results, it appears that ionized carbon can be distributed in clouds of a range of angular sizes along the line

of sight and possess a variety of physical **properties** resulting in detectable carbon line intensity.

However, the above argument raises **more** questions, If the carbon **lines** arise in the neutral gas, probably within a low-excitation **PDR** with temperatures ranging from **80 to 250 K** (and possibly **20 K**), then why are they not detected from many **more** directions in the Galaxy ? It appears natural to think of the existence of stronger carbon lines from directions which show high **H I** optical depth or high ^{12}CO emission. However as discussed in **Sec 5.4.4**, this is not always the case. At this point, it may be useful to note that low-frequency observations have detected carbon lines with **line-to-continuum** ratios ranging **from** a few times 10^{-4} to a few times 10^{-3} . It is a puzzle why the observed optical depths should be limited to **this** narrow range of values. It appears certain that lines very much stronger than a few times 10^{-3} are not **common**. However, the lower limit is **defined** by the sensitivity of the observations conducted till date. Hence, lines intrinsically weaker than few times 10^{-4} might possibly exist and would require more sensitive observations to detect them. In **Sec 5.4.4**, **we** mentioned the **case** of G30+00 from which, **inspite** of a large **H I** optical depth, no carbon recombination line **was** detected **near 328 MHz**. Another such interesting direction is towards the extragalactic source **3C123**. This direction, shows a high **H I** optical depth (~ 2.5). However, no recombination lines near **318 MHz** ($n \sim 274$) (Payne *et.al.* 1984) **have** been detected down to an optical depth limit of 3×10^{-4} . In their recent paper, PAE94 explain that this non-detection could be due to the slightly higher temperature of the **H I** clouds in **this** direction which render the lines undetectable. However, from our modelling, **we** find that a range of temperatures (**80 – 250 K** in the warm models) for the carbon line-forming regions can give rise to detectable peak optical depths in the range $10^{-3} - 10^{-4}$ for a certain range of electron densities, If pressure equilibrium with **H I** gas is assumed, then the electron densities of the partially **ionized** gas is constrained to lie between **0.005** and **0.007 cm^{-3}** assuming a depletion factor **of 0.5** for carbon. This implies atomic densities of $n_{\text{H}} \sim 50 \text{ cm}^{-3}$ in the **H I** gas. Larger electron densities would cause the gas to move out of pressure equilibrium with **H I** and probably into a transitory phase. On the other hand, smaller electron densities ($n, < 0.003 \text{ cm}^{-3}$) require extremely long pathlengths through the partially ionized gas to generate the observed line intensities. Therefore, if such electron densities existed in the partially ionized gas then also the recombination lines would be undetectable. Hence it appears that detectability of the low-frequency recombination lines is a sensitive function of temperature, electron density and the **size** of the line-forming region. **Only** a subset of the range of values possible for these parameters has been so far accessible through

low-frequency recombination lines of carbon.

As discussed in this section, the present low-frequency carbon recombination line observations and modelling of data have shown that various combinations of temperature, electron density and cloud size are capable of giving rise to detectable carbon lines in the Galaxy. Moreover, the physical properties of the partially ionized gas in the inner Galaxy are remarkably uniform. Surprisingly, these lines which are so widespread in the inner Galaxy ($l < 20^\circ$) appear to be difficult to detect in the outer Galaxy except towards a few directions ($l = 63^\circ \& 75^\circ$). The reason could possibly lie in the cloud sizes. Alternatively since our observations have shown that the clouds in the inner Galaxy are $\geq 2^\circ$, the non-detectability could be due to the different physical conditions that may exist in the PDRs in the inner and the outer Galaxy.

5.6 On the Common Origin of Low-frequency Carbon Recombination lines and [CII] $158\mu\text{m}$ line emission

The [CII] $158\mu\text{m}$ line is a result of the radiative decay of the collisionally-excited fine-structure transition, $^2P_{3/2} \rightarrow ^2P_{1/2}$ in ionized carbon. The recombination lines, on the other hand, are a result of the electronic transitions of an electron which has recombined with a carbon ion to an excited state. Both the processes involve ionized carbon and hence it is possible that the same carbon atoms are responsible for both the lines. Moreover, there is another factor which strongly suggests that both the lines may arise in the same medium. This is dielectronic-like recombination process first suggested by WWC80. This process influences the energy level populations in carbon as explained in the previous sections and involves the $^2P_{3/2} - ^2P_{1/2}$ transition which gives rise to the $158\mu\text{m}$ emission. The two lines are thus, intimately related and it seems natural to look for a correlation between the two intensities. However, it should be kept in mind that although dielectronic-like recombination process is one excitation mechanism for the fine-structure line, it need not be the only one. There could be other mechanisms which excite the fine-structure line and hence the two lines may not show a strong correlation. Recent advances made in infrared observations have extensively detected the [CII] $158\mu\text{m}$ line from the Galaxy and it can be inferred that a wide range of physical conditions seem to be conducive to the formation of the finestructure line. C^+ is found to exist in both neutral and ionized regions. Shibai *et al.* (1991) concluded from their balloon-borne experiments that the diffuse [CII] emission of the Galactic plane comes from the diffuse gas whereas Bennett & Hinshaw (1993) showed that the [CII] emission measured with COBE/FIRAS may originate in the PDR. Petuchowski

& Bennett (1993) and Heiles (1994), in separate studies, analysed the [CII] data and studied its correlation with the various possible sites of origin. Both the studies find that the extended low-density warm ionized medium (ELDWIM) is the main global contributor to the $158\mu\text{m}$ fine-structure emission line especially in the Galactic interior. Heiles (1994) argues that the next contributor is the CNM and the last is the PDR. On the other hand, as the models presented in the previous section indicate, the carbon recombination line emission is detected only from the neutral medium and not from the ELDWIM. Since, the major contributor to the two species of lines seems to be different, it may not be meaningful to interpret any correlation which may exist between the fine-structure line and recombination lines at this stage.

5.7 Summary

In this chapter, we have discussed the association of the ionized carbon seen in low-frequency recombination lines with other components of the interstellar medium and derived the probable physical properties of this partially ionized gas. Carbon recombination lines at 34.5 MHz were detected from all the observed positions in the inner Galaxy ($l < 17^\circ$) with an angular resolution of $21' \times 25^\circ$. Since the beam is large in one direction, to obtain some constraint on the size of the region that contributes to the detected lines, we studied the distribution of non-thermal continuum at 34.5 MHz over the beam area. Except for two directions, the continuum emission appears to be fairly uniform over the beam. This uniformity indicates that unless the line-forming gas is distributed over the entire beam, there will be beam dilution at 34.5 MHz. The observations with the Ooty Radio Telescope, conducted with two angular resolutions, showed that the line-forming region is at least $\sim 2^\circ$ in extent. VLA observations of one of the inner Galaxy regions constrained the fine structure in these line-forming clouds to be on scales $> 10'$.

The widths of the lines observed at 34.5 MHz and 328 MHz are remarkably similar indicating that pressure or radiation broadening is not the cause of the line widths. The common origin of the line width is most likely differential Galactic rotation. From the Galactic rotation model, it was deduced that the line-forming gas is distributed between Galactocentric distances of 4 & 7.5 kpc. A comparative study of the radial velocities of the observed carbon recombination lines with those of HI emission, HI absorption and ^{12}CO showed that the carbon line regions are more spatially localized. Carbon recombination lines are detected at radial velocities close to the velocities at which peak HI optical depth and ^{12}CO emission are observed indicating that the ionized

carbon is likely to be associated with either or both neutral H I and H₂ regions in the ISM. However, non-detection of carbon lines towards other directions with even larger H I optical depths suggests that other factors influence the detectability of the recombination lines.

The lineforming regions were modelled using our data at 34.5 & 328 MHz and also the data at 76 MHz from Erickson, McConnell & Anantharamaiah (1995). The process of dielectronic-like recombination which significantly modifies the level populations was included in the calculation of the level populations in carbon. The computer code by Salem & Brocklehurst (1979) modified by Walmsley & Watson (1982) and Payne, Anantharamaiah & Ericksan (1994) was used for this purpose. For modelling the line regions, temperatures typical of (1) molecular (H₂) gas ($T_e \sim 20$ K) and (2) atomic (H I) gas ($T_e \sim 30 - 300$ K) were considered. The low temperature models were able to explain the observed variation in optical depth with frequency if the cloud sizes are $> 4^\circ$. However these models predict sheet-like geometry for the ionized carbon. Such a geometry seems incompatible with observed line widths. The warm gas models were able to explain the observed optical depths towards several positions if the cloud sizes were $\ll 25^\circ$. Warm gas models gave reasonable pathlengths in the range 0.2 - 2 kpc and this could account for the line width in terms of Galactic rotation. The regions were constrained to be in pressure equilibrium with the interstellar medium. It therefore appears likely that the observed low-frequency recombination lines of carbon may arise in the widespread cold neutral H I in the Galaxy. It may be possible to identify these regions with the low-excitation photodissociation regions (PDR) described by Hollenbach, Takahashi & Tielens (1991) which contain both atomic & molecular hydrogen and encompass a range of physical parameters. Although, the dielectronic-like recombination process in carbon involves the fine structure states, $^2P_{3/2}$ & $^2P_{1/2}$, which give rise to the [C II] 158 μm fine-structure line, we argued that a direct correlation between the low frequency recombination line and the fine-structure infrared line may not be expected.